Lateral offsets and revised dates of large prehistoric earthquakes at Pallett creek, Southern California

Sieh, Kerry

1984

Sieh, K. (1984). Lateral Offsets and Revised Dates of Large Prehistoric Earthquakes at Pallett Creek, Southern California. Journal of Geophysical Research, 89(B9), 7641-7670.

https://hdl.handle.net/10356/79868

https://doi.org/10.1029/JB089iB09p07641

JOURNAL OF GEOPHYSICAL RESEARCH, VOL. 89, NO. B9, PAGES 7641-7670, SEPTEMBER 10, 1984

Lateral Offsets and Revised Dates of Large Prehistoric Earthquakes at Pallett Creek, Southern California

KERRY E. SIEH

Division of Geological and Planetary Sciences, California Institute of Technology, Pasadena

Recent excavation and new radiocarbon dates of sediments at Pallett Creek are the basis for new conclusions regarding the late Holocene history of the San Andreas fault. Systematic dissection of a 50-m-long, 15-m-wide, 5-m-deep volume of earth, centered on the fault, enables documentation in three dimensions of fault patterns, lateral offsets, and vertical deformation associated with large earthquakes of the past. The excavations expose evidence for 12 earthquakes that occurred between about 260 and 1857 A.D., with an average recurrence interval of about 145 years. Prehistoric slip events that occurred in 1720 ± 50, 1550 ± 70, 1350 ± 50, 1080 ± 65, and 845 ± 75 A.D. have lateral offsets that are comparable to those of the most recent great earthquake of 1857. Thus all of these events represent earthquakes of large magnitude. The lateral offsets of two other events, in 935 ± 85 and 1015 ± 100 A.D., are an order of magnitude smaller and may be interpreted in several ways with regard to the size of these events. The new data constrain the average recurrence interval for large earthquakes at this site to between 145 and 200 years but suggest a monotonic decrease in individual intervals to below this range during the past 900 years. On the basis of these data, the probability of a large earthquake with surficial fault rupture at this site is between 0.2 and 5% during 1984 and 7 and 60% by the year 2000.

1. INTRODUCTION

Several years ago I described evidence and reported dates for eight large earthquakes that occurred in the 1300 years before 1857 A.D., the date of the latest great earthquake in southern California [*Sieh*, 1978*a*]. These events were revealed in excavations across the San Andreas fault at Pallett Creek, about 55 km northeast of downtown Los Angeles (Figure 1*a*). Using several radiocarbon (^{14}C) age determinations for various faulted late Holocene layers, I estimated an average recurrence interval of about 160 years between these nine events.

Several limitations plagued the early study at Pallett Creek. First, large uncertainties in the radiocarbon dates translated into large uncertainties for the dates of the individual earthquakes. Thus one could not assess whether variations in recurrence intervals were due to the imprecision of the radiocarbon analyses or to actual variations in the length of time between earthquakes. Second, the sizes of the individual events were difficult to assess because right-lateral dislocations associated with each event could not be measured in the few, isolated, narrow trenches excavated for that study. I did use vertical deformational patterns to assess the size of each prehistoric event relative to the 1857 event, but this involved the assumption that deformation in the vertical plane has occurred in the same proportion to that in the horizontal plane during each of the earthquakes.

In this paper I present new radiocarbon dates and recalculate the date of each earthquake. I also report new measurements of horizontal fault slip associated with most of the earthquakes. In order to reassess the dates of each earthquake recorded at Pallett Creek, I collected additional samples of peat and charcoal from various stratigraphic horizons. Dates from these samples were used in combination with those I reported earlier [*Sieh*, 1978*a*] to recalculate the dates of each earthquake. In addition, excavation of trenches well below the base of the earlier trenches enabled identification and dating of three older earthquakes that had not been known. To determine lateral offsets associated with the large earthquakes at Pallett Creek, I systematically excavated a volume of earth that is roughly 50 m long parallel to the fault, ≥ 15 m wide, and 5 m deep (Figure 1*c*). Most of the data from the excavated volume come from about 50 vertical exposures oriented nearly at right angles to the fault. Excavation began with a 2-m-wide, 2-m-deep, 20-m-long swath cut across the fault. The two walls of this cut were cleaned, and several points on each wall were located with respect to a reference grid that had been surveyed by transit, rod, and tape prior to excavation. A string grid composed of 1-m squares was then constructed on each exposure (e.g., Figures 2 and 3). The stratigraphy and structure of each square was then documented by color photographs and written descriptions of strikes and dips as well as unit thicknesses, textures, and colors. Documentation of each major exposure required approximately half a day.

Once the walls of the initial excavation were documented, the cut was widened. In this manner the initial exposures were destroyed, but a fresh wall was exposed. After documentation of this new exposure was completed, the excavation was widened further to expose yet another vertical surface. After the first 2-m-deep tier was 10 m or so wide, excavations to a lower, 4-m-deep tier were undertaken. Figures 2 and 3 illustrate walls exposed in the two tiers. In most critical areas the spacing between the mapped vertical exposures was <1 m, and in a few places small horizontal surfaces were prepared and mapped. Documentation of more than 130 exposures within the excavated volume required two summer field seasons (1979 and 1980).

Taken together, the exposure records constitute a three-dimensional latticework of structural and stratigraphic information. Throughout the latticework are major and minor faults and fissures; sandblows, anticlines, synclines, and monoclines; and mappable variations in the textures, colors, and thicknesses of units (for example, see Figures 2 and 3). Dozens of offsets and deformations of various ages are apparent at various levels. Although a large volume of geological record was destroyed in the process of collecting these data, volumes several times as large remain unexcavated within the flood-

Paper number 4B0612.
0148-0227/84/004B-0612$05.00

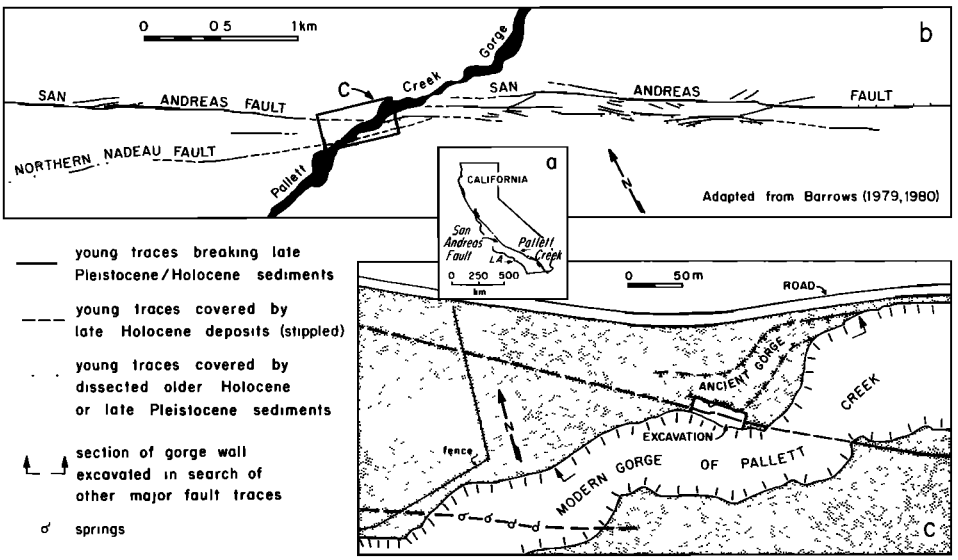

Fig. 1. (*a*) Location map showing Pallett Creek at the San Andreas fault about 55 km northeast of Los Angeles (LA). (*b*) Map showing Pallett Creek and nearby traces of San Andreas fault and Northern Nadeau fault. The Pallett Creek excavations (in center of box labeled "c") are at the northwest edge of a major step-over in the active fault trace. (*c*) Detail of active trace of San Andreas fault. Excavation described in this report is between ancient and modern gorges of Pallett Creek.

plain of Pallett Creek to the northwest and southeast. These remain untouched and preserved for future investigators.

Before considering the effects of ancient earthquakes, one must be familiar with the stratigraphic section in which the effects are displayed. The sediments of the Pallett Creek section are late Holocene peats, clays, silts, sands, and gravels of biological, fluvial, and aeolian origin. A detailed description of the geographic and geologic setting of the sediments is given by *Sieh* [1977, 1978*a*]. Figure 4 is a generalized columnar section of the part of the section that occurs above the present water table. Most numbered units are continuous and recognizable throughout the excavation. These sediments have accumulated at relatively uniform rates during the past 2000 years. Major entrenchment of the section by Pallett Creek occurred in about 1050 A.D. and again in about 1910. Except for scour and fill related to these two major events the sediments are nearly devoid of evidence for erosion. Apparently, the fluvial and aeolian clastics aggraded without intervening periods of even local erosion.

2. Basic Structure and Structural History

Pallett Creek crosses the San Andreas fault zone near an en echelon step in the late Holocene fault (Figure 1*b*). Thus one might question whether or not the excavations exposed all major branches of the fault. Fortunately, it has been possible to demonstrate that only one principal fault exists at the longitude of the site. Northwest of the site, geological mapping of Cenozoic rocks and geomorphic features defines a narrow and relatively simple main trace [*Barrows*, 1979, 1980]. This solitary main trace is the one revealed in the excavations.

Exploratory excavations along the northern wall of the modern gorge of Pallett Creek (between arrows on Figure 1*c*) prove that within about 100 m of the site no other faults have slipped during at least the past millenium.

About 100 m southwest of the main fault is the Northern Nadeau fault, a secondary structure which probably has been active along at least part of its length during the late Pleistocene and perhaps the Holocene epochs. *Barrows* [1980], however, shows dissected older alluvium (Qoa) less than a kilometer to the northwest of the site that is unbroken by this fault. Thus this discontinuous secondary fault cannot have experienced more than a small fraction of the late Holocene slip experienced by the main trace of the San Andreas.

From 100 m north of the main trace and continuing northward, are exposures of Tertiary sandstone and conglomerate that are devoid of major youthful faults [*Barrows*, 1979, 1980]. Faults that break Pleistocene gravels southeast of Pallett Creek cannot be traced northwestward across the creek in these deposits (Figure 1*b*). Thus there is good reason to believe that the main trace of the San Andreas fault exposed in the excavation has experienced many times more slip than any other late Holocene trace in the fault zone.

Figures 2 and 3 display the San Andreas fault within the excavation. The trace visible in the center of Figure 2 has been more recently active than the traces toward the left (northern) margin. Layers as young as unit 81 (~1700 A.D.) and 88 (1857) have been offset along the central trace, whereas the more northerly trace ends abruptly at unit 68 (~1550 A.D.) and is buried by younger units. This fault last moved in about 1550 A.D.

Figure 3 shows three major faults that cut the sediments. Near the lower right (northern) margin of the photograph is a fault that breaks beds below and including unit 38 (~850 A.D.). In the center of Figure 3 is a fault which breaks only those beds below and including unit 61 and terminates upward into a large sandblow pit (labeled T). Nearer the left (southern) margin of the photograph is the youngest fault, which breaks all units in the lower exposure and all beds through unit 88 in the upper exposure. Detailed mapping was necessary to prove that all three major faults are truncated abruptly at their upper terminus in these and subparallel exposures. Such complete documentation was the principal focus of *Sieh* [1978*a*] and would be too cumbersome to include in this report. I ask for the reader's trust, then, in my observation

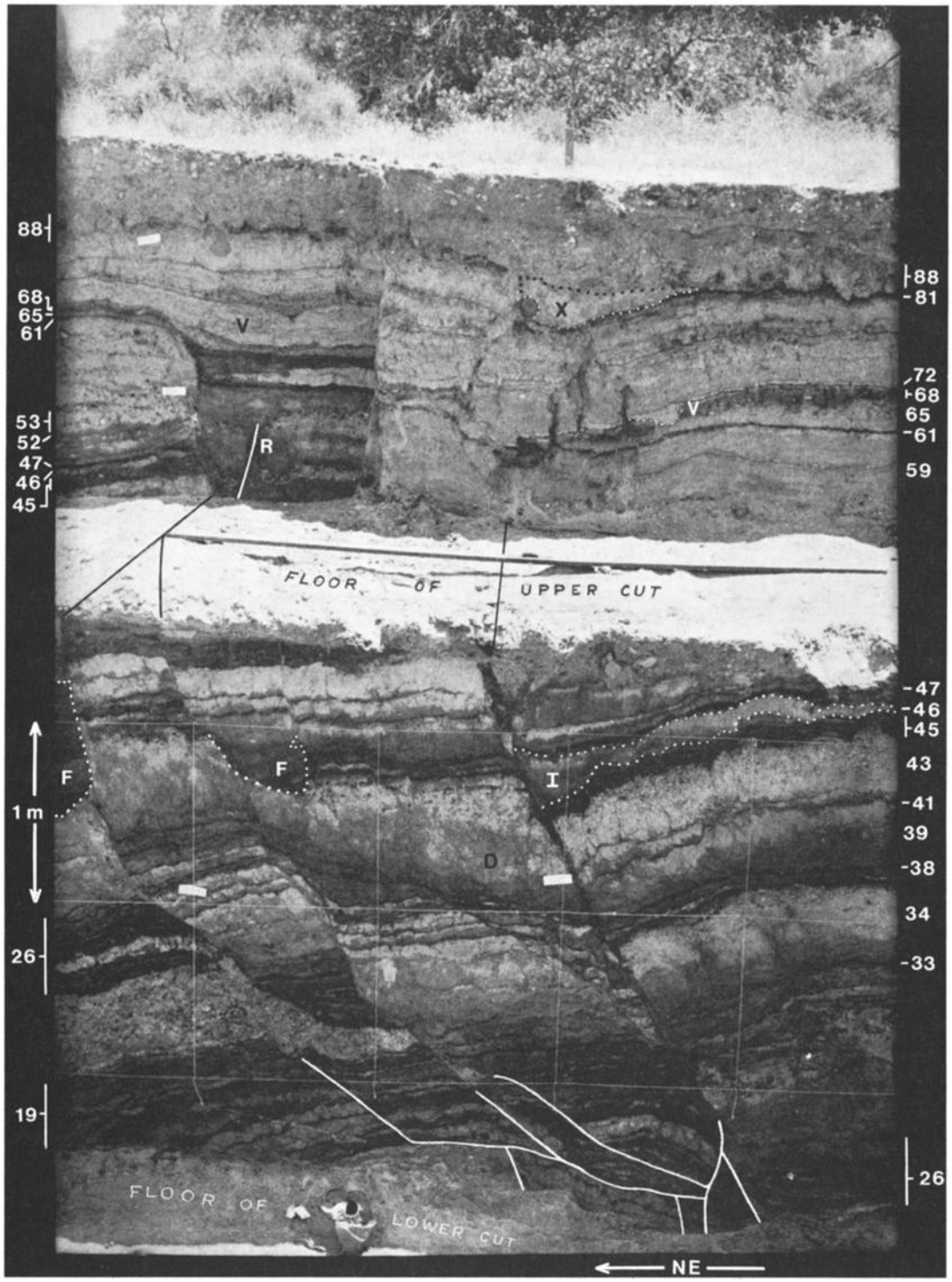

Fig. 2. Two typical vertical exposures at Pallett Creek display a 1700-year-long record of sedimentation and earthquakes. One-meter string grid is located relative to a baseline by careful surveying. View is toward the southeast. Numbers on margins indicate various beds. Letters F, I, V, and X indicate sandblows and pits associated with seismic events F, I. V, and X. Letters D, R, and V indicate evidence for fault slip during events D, R, and V. The nature of this evidence is discussed by *Sieh* [1978*a*]. Leftmost fault has not slipped since unit 72 was deposited about 400 years ago. Centermost fault last slipped in 1857.

of these details. The abrupt upward termination of these faults clearly indicates that the active trace of the San Andreas fault zone has shifted from the northern trace in this figure (active until about 850 A.D.) to the central trace (active until about 1350 A.D.) to the southern trace (active as recently as 1857).

The late Holocene evolution of the major traces of the San Andreas is summarized in Plate 1. Detailed description and discussion of these patterns of deformation follow in the next section. The only point to be made now is that the fault traces have migrated southwestward with time. Inspection of the

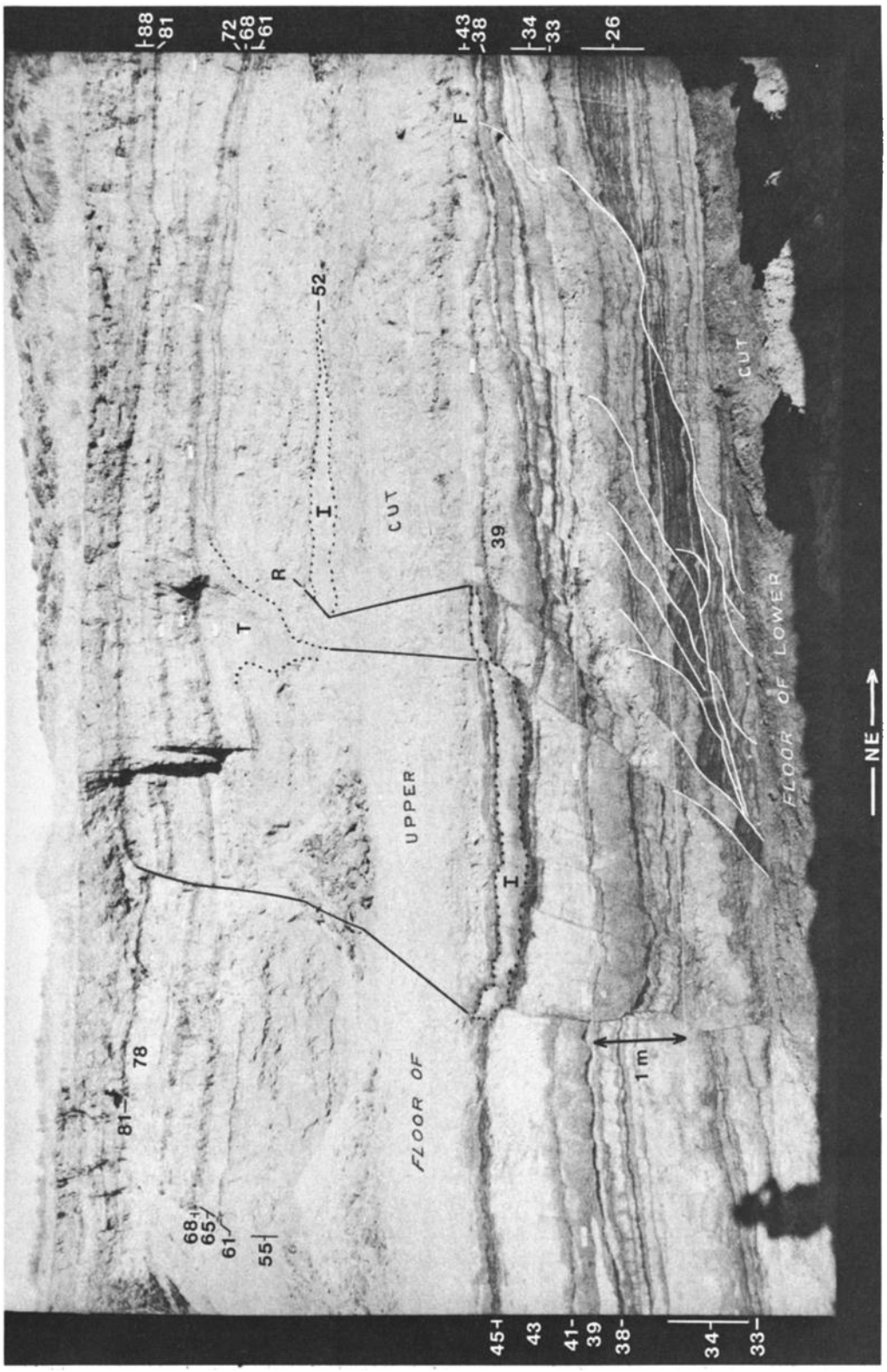

Fig. 3. Two other typical exposures display sediments and structures at Pallett Creek excavation. View toward the northwest. Activity progressed from the northernmost fault (labeled "F" on the right) to the centermost faults to the southernmost fault (on the left) during the past 1000 years.

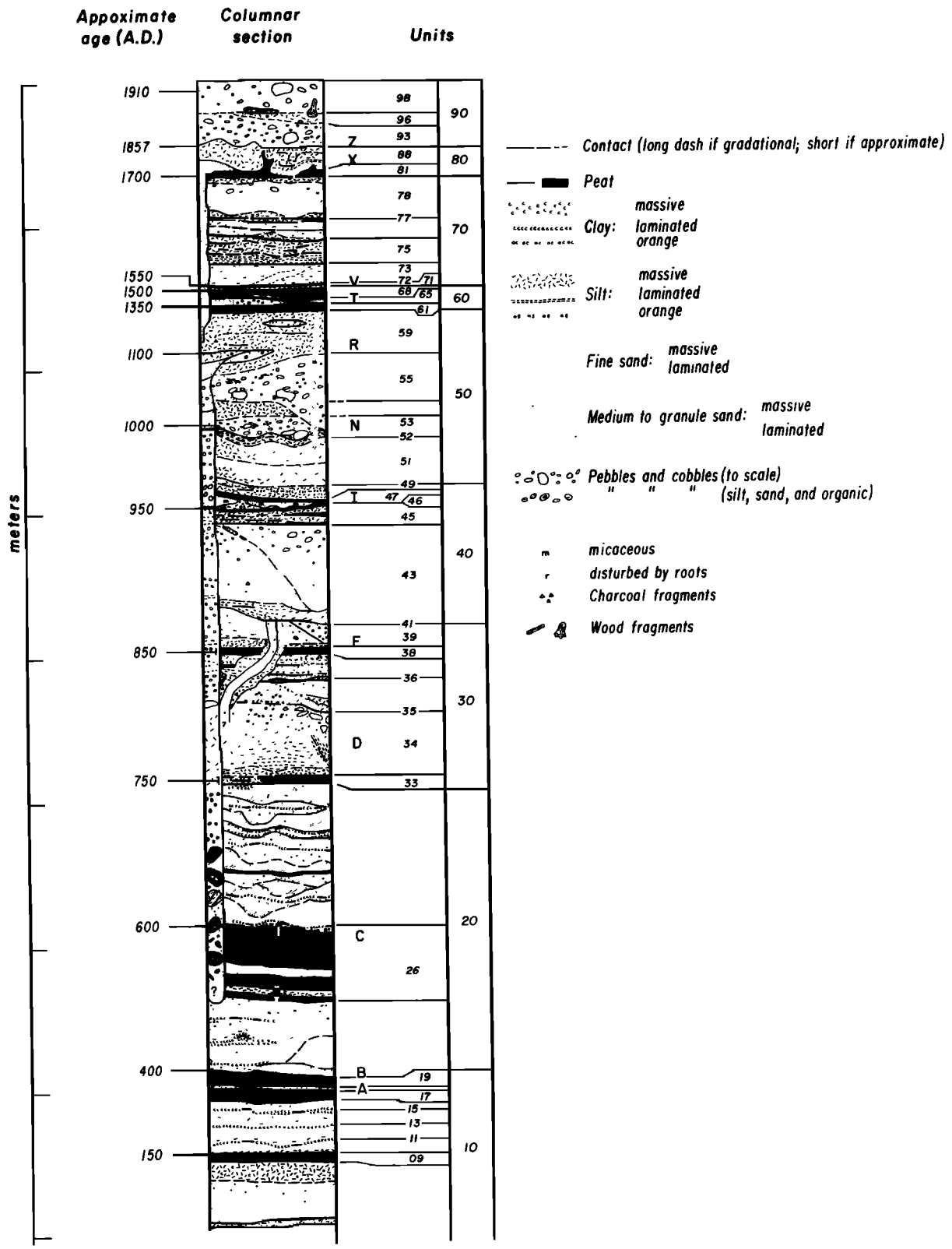

Fig. 4. Generalized columnar section of the late Holocene sediments of Pallett Creek within the excavation. Individual beds are labeled numerically as by *Sieh* [1978*a*]. Each capital letter rests upon the stratum that constituted the ground surface at the time of a particular earthquake. Dates based on radiocarbon analyses are rounded to nearest 50 years.

main rupture locations relative to the reference lines reveals that earlier events involved rupture on more northeasterly planes than later events.

The section that follows makes extensive use of isopach and structure contour maps. Figure 5 illustrates how such maps help determine the vertical deformations associated with particular earthquakes. Isopach maps have proven especially useful in defining the style and magnitude of deformation for

several prehistoric events because at the Pallett Creek site most beds have been deformed and offset more than once. Of course, such maps represent deformation only to the extent that (1) the isopached units had rectiplanar upper surfaces after deposition and (2) no appreciable erosion of deformed surfaces occurred prior to burial by the isopached unit. These conditions are met by several units discussed in the text that follows.

3. THE EVENTS

3.1. *Events X and Z*

3.1.1. *Fault geometry.* Disassociation of the effects of event Z from those of event X is difficult for reasons that will be discussed below. The effects of these two events are therefore discussed together throughout this and most of the following two sections.

Numerous exposures reveal that the main fault rupture during events X (~1720 A.D.) and Z (1857) was continuous across the entire excavation (panel "X and Z,", Plate 1). Lateral offsets discussed below indicate that the portion of the main rupture northwest of the major bend at point "d" (panel X and Z, Plate 1) was a new fault at the time of event X, whereas the portion southeast of "d" had been active previously. (Localities are lettered alphabetically, from left to right, beginning with this panel.) Several secondary faults slipped during events X and/or Z. The fault labeled "b" formed a join between older faults visible in the subsurface, and fault "g" was a new fault during event X. Minor faults in the vicinity of "c" are inferred to be dextral and probably represent deformation of this area as it moved toward the major bend in the main trace. Two sandblows formed during event X, the more southerly of which is discussed in detail by *Sieh* [1978*a*, p. 3923], but none formed during event Z in 1857. A spring at point "f" commenced flowing after event Z, and a pail and wooden planks discovered in the sands of the spring are evidence that water was drawn from the spring by settlers in the 1800's.

3.1.2. *Fold geometry.* The combined vertical deformation pattern of events X and Z is also shown in Plate 1 (panel X and Z). It is derived from the structure contour map of unit 81 (Plate 2). This peaty bed was deposited during the late seventeenth and/or early eighteenth centuries upon a ground surface with a gentle (~3°) eastward dip. (Evidence that unit 81 was rectiplanar prior to event X is discussed by *Sieh* [1978*a*, p. 3923, Figure 19].) Superimposed upon this original, uniform gradient are irregularities that principally reflect deformation of events X and Z. In addition to the southwest facing scarp of variable height along the main fault trace, several anticlines and synclines formed during events X and Z. Most notable among these broad folds is a doubly plunging syncline southwest of the main fault and an anticlinal welt northeast of the main fault. Anticlines and synclines trending obliquely to the main trace formed in the northwestern 13 m of the mapped area. These are consistent with an interpretation of broad dextral shear in the area of these small folds, north of the main fault trace, and may indicate that some dextral slip occurred on an older fault (dotted in Plate 1) that dies out more than 1 m below the ground surface.

3.1.3. *Lateral offsets.* Several pieces of evidence indicate that lateral offset along the main fault totals about 4 m for events X and Z, and at one locality this 4-m offset can be shown to be equally divided between the two events.

At the southeastern edge of the map area, three isopach contours of unit 78 are offset 4.4 ± 0.3 m. Plate 3, panel 20, displays those offsets in plan view and Plate 3, panel 1, illustrates the offsets in the plane of the fault (diamonds near 33 and 38 m). Several meters farther northwest, facies boundaries of unit 78 (circles numbered 1, 2, and 3) are offset about 4.2 m (Plate 3, panels 1 and 15).

Near the center of the cut (near 16 and 20 m) another facies boundary, the edge of a gravel stringer of unit 78 (circles), is offset about 3.9 m (Plate 3, panels 1 and 15). Near the western edge of the area, all features within units 34 to 78 are offset about 3–4 m (Plate 3, panels 1, 3, 7, 11, 14, 15, and 17). This indicates that the fault at this location experienced dextral slip only during events X and Z. Fault planes which slipped during

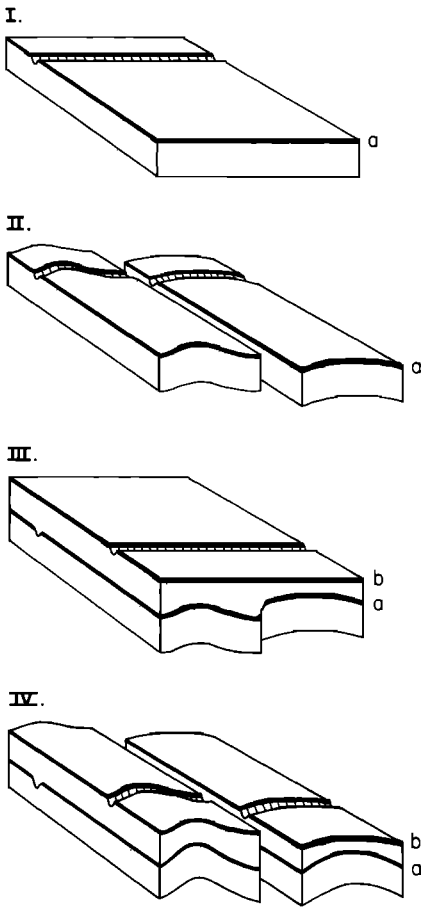

Fig. 5. Structure contour and isopach maps can preserve the pattern of surficial deformation resulting from an earthquake. I, small gully has cut sandy layer overlain by peat bed, "a." II, faulting during large earthquake has deformed and offset the beds and gully. Note right-lateral strike slip, small component of dip-slip faulting, and mild folding. A topographic map of the ground surface after this earthquake and before the next would represent the vertical deformations of the earthquake. III, beds deposited upon these deformed beds in the decades following the earthquake are a "mold" of the deformed ground surface they mantle. An isopach map of these overlying beds would contain the same structural information as a structure contour map of the deformed surface. IV, beds after second large earthquake. New ground surface, "b," is now faulted and deformed. Topographic map of this newly deformed surface would reflect these new deformations. However, the surface of the older peat, "a," has now been deformed twice, so structure contours drawn on it would represent the accumulated effects of both events. The isopach map of the sand layer between "a" and "b" would still reflect principally the vertical deformation of the first event.

event I, N, and/or R (diamonds and inverted triangles in Plate 3, panels 1, 11, and 17) are offset only about 3 m (~2.5 m in the plane of Plate 3, panel 1) on this trace. This shows that either an episode of sinistral slip occurred during event N and/or R or that slip during events X and Z decreased from 4 m at the surface to 2.5–3 m at a depth of several meters. The first explanation is not plausible because evidence presented below indicates (1) that large right-lateral slip occurred at the site during event R and (2) that event N involved no more than about 10 cm of lateral slip.

3.1.4. *Partitioning of slip and deformation between events X and Z.* Comparison of the magnitude of slip and deformation during event Z (1857) with that of prehistoric events is critical to assessing the size of these earlier events. One must disassociate the effects of event Z (1857) from those of event X in order to make these comparisons. This has been quite difficult at the Pallett Creek site because of both a stratigraphic and a structural peculiarity. First, unit 88, which was the youngest unit in 1857, has an ill-defined upper surface. Thus it is impossible to produce a structure contour map that reflects only the deformation associated with the 1857 earthquake. Second, most fault scarps associated with event Z involve monoclinal flexuring and strike-slip warping. Sharp dislocations are uncommon. In several exposures, unit 88 does not even appear to be broken by event Z. This faulting over a broad zone has made correlation of offset iospachs impossible.

Nonetheless, rare, but conspicuous faulting of unit 88 against 78 [e.g., *Sieh*, 1978*a*, trench 10] and deformation of sandy fluvial beds of unit 88 across the fault offer compelling evidence for event Z and imply that event Z must be the latest major event at Pallett Creek. In a few exposures the scarp and other vertical deformation that resulted from event Z are nearly identical in style and magnitude to the deformation produced during event X [e.g., *Sieh*, 1978*a*, Figure 22].

It is indeed fortunate that at the southeastern edge of the excavated area a suite of offset reference features indicate that the 1857 earthquake was associated with 2 m of dextral slip (see reclining rectangles and upright rectangles in Plate 3, panel 1, near 31 and 33 m). These data, which are discussed below, demonstrate that event Z had a dextral offset of 2 m. Figure 6 illustrates the complex development of the 2-m offsets during event Z based on careful reconstruction of many vertical exposures. Figure 7 depicts in three representative cross sections the features that were offset 2 m in 1857. The overall timing of the faulting and slumping events shown in these figures is not deduced strictly from structural relationships but also from the relative amount of dextral offset of three features. The reverse faulting and the initial slump must have occurred almost simultaneously because the reverse fault cusp (vertical rectangles), the deepest parts of the initial slide mass (horizontal rectangles), and the slide headscarp (rectangles with dot) are all offset about 2.1 m (Plate 3, panel 1).

3.2. *Event V*

3.2.1. *Fault geometry.* Faulting attributable to event V occurs across the entire width of the excavation, and its style is similar, but not identical to, faulting of events X and Z. Event V shares with events X and Z a majority of the straight central fault trace ("k" to "o" in panel V of Plate 1). Southeast of point "o," however, the event V rupture steps left (i.e., eastward) by way of a "scissor" fault onto another fault ("p") (the prominent fault on the left side of Figure 2). This fault produced a 25- to 40-cm-high scarp on unit 68, which was left virtually intact and uneroded until it was preserved by burial under units 71, 72, and other strata. A representative cross section of the fault "p" is displayed on the left side of Figure 2, in which one can see that the dip of the fault decreases progressively to a depth of 4 m, where the fault terminates against the younger, main fault of events X and Z.

At point "k" is a discontinuity in the surficial trace of the fault. Northwest of the discontinuity, fault "i" is expressed as a southwest facing fault scarp and monoclinal scarp. A similar fault scarp and monoclinal scarp occur at "l." These two faults are connected in the subsurface by fault "j," which is the same reverse fault that is labeled "b" in frame X and Z of Plate 1.

Numerous pits and fissures formed during event V. The pits are filled with fragments of older units and laminated to massive punky silt that is probably of aeolian and sublacustrine origin. The pits do not have vents beneath them and are in areas that, judging from fault geometry, underwent severe compressive deformation during event V. For example, two

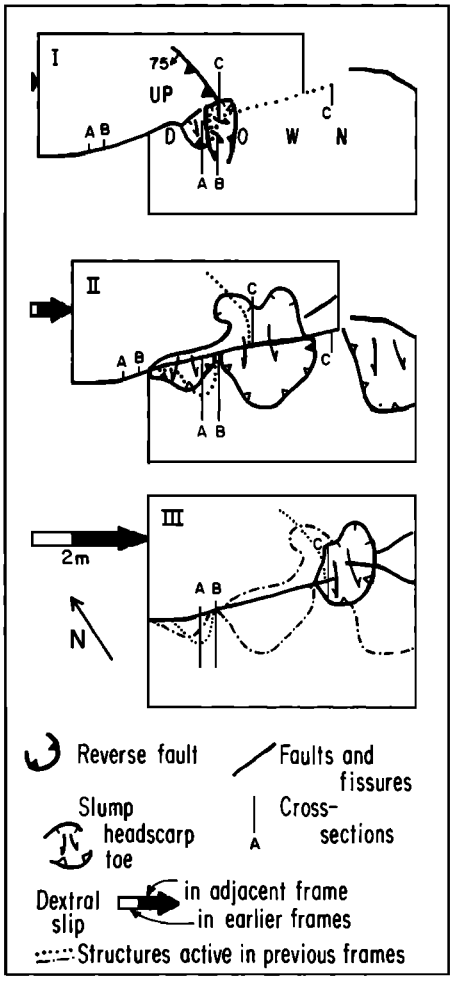

Fig. 6. Map of sequential development of faults and slumps during event Z (1857). I, event Z faulting begins with formation of reverse fault cusp at eastern end of main strike-slip fault. Incompetence of water-saturated, uplifted mass within cusp results in rapid slumping of portion of hanging wall. II, Main fault propagates through cusp and slump and offsets each about 70 cm (note dots). Shallow slump moves off upthrown northern block onto lower, southern block. III, additional 1.3 m of slip occurs, leaving 2-m total strike-slip offset. Small slump moves across fault after fault slip is completed. See Figure 7 for representative cross-sectional views A, B, and C.

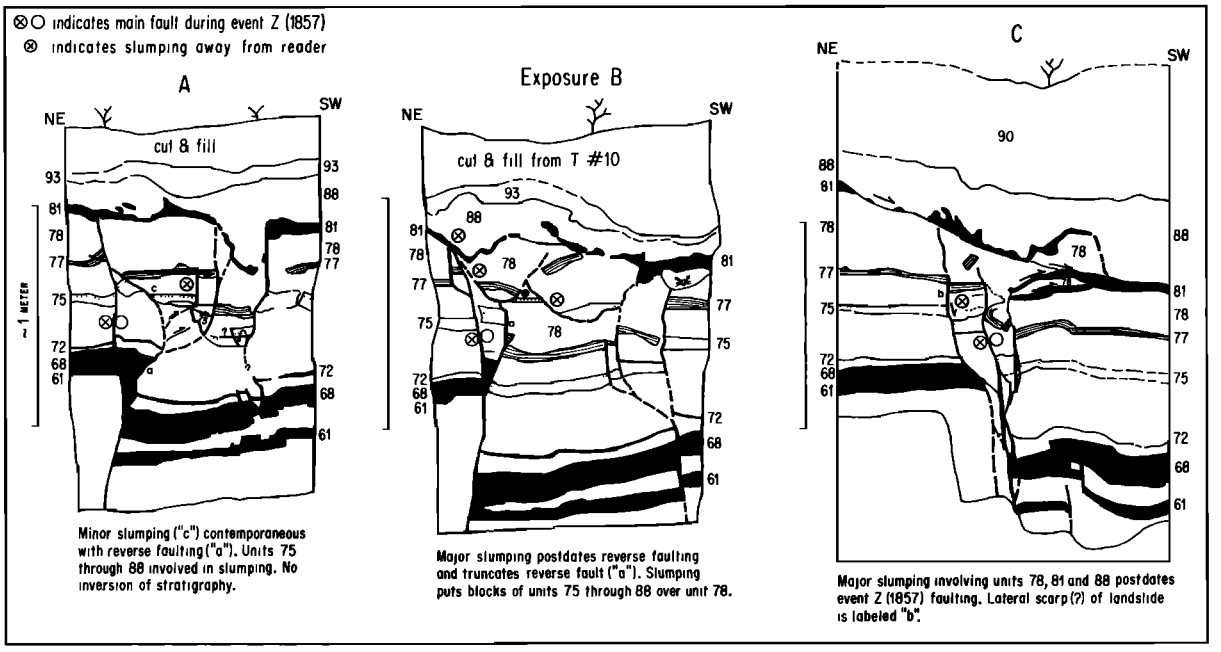

Fig. 7. Vertical exposures A, B, and C (exposures 131.0, 131.3, and 133.45 on index panel of Plate 1) illustrate faults and slumps of Figure 6, in cross section. Cusp-shaped reverse fault of Figure 6, panel I, is labeled "a" in exposures A and B. Minor slumping away from reader (solitary circled cross) occurred at the same time as the reverse faulting in exposure A. In exposure B, major slumping (three solitary circled crosses) occurred after the reverse faulting. The northern lateral scarp of this slump is labeled "b" in exposure C. Later slumping of Figure 6, panels II and III, involves units 81 and 88 in exposure A and units 78, 81, and 88 in exposure C and truncates earlier structures.

large pits, one 4 m west of "k" and one 4 m southeast of "i" formed adjacent to a discontinuity in surficial faulting (note that the pit west of "k" was moved 4 m west of "k" during events X and Z). The pits probably formed explosively by expulsion of pore fluid from sediments within a meter of the event V ground surface.

3.2.2. *Fold geometry.* I demonstrated earlier [*Sieh*, 1978*a*, p. 3923 and Figure 19] that unit 70 completely buried the vertical deformations associated with event V. That is, the upper surface of unit 70 was a uniformly southeast dipping plane that did not reflect the irregular topography produced during event V. Thus the isopach map of unit 70 (Plate 5) is a "mold" of the ground surface that existed just after event V. In other words, areas where unit 70 is thick represent topographic lows, whereas areas where unit 70 is thin represent topographic highs in the post–event V topography. This isopach map can be regarded as a mold of event V deformations because the surface just prior to event V was relatively smooth and uniform and did not reflect deformation associated with the latest event that occurred prior to V. Unlike the structure contour map employed in discussing vertical deformation of events X and Z, the isopach map of Plate 5 has no regional slope superimposed upon the deformations. Thus one may interpret it directly as deformation.

A comparison of deformations during event V with those of events X and Z (Plate 1) reveals one striking similarity: northeast of the fault traversing the central two thirds of the map area is an anticline running subparallel to the fault. The event V anticline has a peak-to-trough amplitude of about 30 cm at point "m" (Plate 5), whereas the anticline of events X and Z has an amplitude of about 50 cm at the same locality ("e," Plate 2). Other similarities in deformation are less impressive but, nevertheless, are noteworthy: a 15-cm-high anticline at "h" in Plate 5 is similar to a 25-cm-high anticline at "a" in Plate 2; a 10-cm-high anticline at "k" in Plate 5 is remarkably similar to the 20-cm-high anticline at "d" in Plate 2 but of opposite plunge. Other event V features have no comparable features from events X and Z. With only one exception these features are near event V faults that have no counterpart during events X or Z. The steep slope at "p" in Plate 5, for example, is associated with dip slip on the fault labeled "p" in Plate 1, panel V; this fault did not produce a steep scarp during X and Z. Likewise, event V faults adjacent to basins at "i," "l," and "n" in Plate 5 were not active during X and Z. The one major exception is the structures southwest of the main fault in the central third of the map area. During events X and Z a 70-cm-deep syncline formed parallel to and southwest of the fault (Plate 2). The main fault was active during X and Z as well as during V, and yet the adjacent structures are quite dissimilar. During event V, no such syncline formed, but rather, a group of E-W trending synclines and anticlines appeared (Plate 5). Possibly, these are indicative of dextral warping adjacent to the event V main fault.

The comparison of faulting and patterns of vertical deformation in panels "X and Z" and "V" of Plate 1 indicate that within the map area, event V was the most geometrically complex of the latest three events. Nevertheless, the amplitudes of anticlines that formed during V are only about half as great as those which resulted from vents X and Z combined. If the combined deformational amplitudes of events X and Z were split equally between event X and Z, all three events, V, X, and Z would be judged as approximately equal in size.

3.2.3. *Lateral offsets.* Lateral slip associated with event V can be measured along two separate fault segments: "i" and "p" (Plate 1, panel V).

Event V was the latest event to involve rupture of fault "p" (panel V, Plate 1) and the scissor fault connecting it to the central segment. Therefore one need not subtract slip associ-

ated with later events X and Z. Isopach contours of units 65 and 68, which were deposited in the ~200-year period prior to event V, reveal 1.5 m of event V slip on this fault. The 15- and 20-cm contours are particularly well constrained to a 1.5-m offset (see triangles in Plate 3, panels 2 and 10). Restoration of this amount also juxtaposes the 25-cm contour south of the fault with a 25-cm-deep fissure north of the fault. At the same locality a facies boundary of unit 65 also yields a 1.5-m dextral offset (see reclining triangles in Plate 3, panels 2 and 13), although it is not well constrained because of unfortunate placement of the vertical exposures. The vertical component of the slip vector here is 20–40 cm, as evidenced by the relative elevation of the two offset markers discussed above and the change in thickness of unit 70 across the scarp (Plate 5).

A sandblow pit bisected by event V faulting in the northwestern part of the site yields an offset value for event V, also (see inverted triangles in Plate 3, panels 2 and 3). The pit walls cut units 61 and 59 but are capped by unit 68. Therefore the pit formed within the event T fault zone during or just after event T faulting occurred. The pit is offset 0.8 ± 0.2 m along the event V trace. The only event on this fault to postdate the formation of the sandblow pit is event V. Therefore event V is associated with 0.8 ± 0.2 m of dextral slip on this fault. The numerous event V folds oriented transversely to this fault (see Plate 5) suggest that a substantial but unknown amount of strike slip also occurred as warping within a 15-m-wide zone centered on the fault.

In conclusion, event V resulted in 0.8–1.5 m of dextral slip on faults within the excavation. Trace "i" sustained about 1 m and is adjacent to folds that may be evidence of additional dextral shear. Trace "p" sustained about 1.5 m of right-lateral slip. Slip on major faults at Pallett Creek during event V was 50–75% as large as slip during either event X or Z. Therefore I concluded that the event V was a large event, similar in size to event X and event Z.

3.3. *Event T*

3.3.1. *Fault geometry.* The pattern of faulting in event T is similar to that of event V. By comparing panels V and T of Plate 1 one can see that the same four principal traces and the same two major en echelon transitions or step-overs were utilized. However, the en echelon transition at the southeastern end of the central trace differs appreciably from the analogous event V feature. During event T the main step-over occurred farther southeast, at the southeast boundary of the mapped area. In the northwestern portion of the excavation the monocline of event V is replaced by an event T fault scarp and sandblow pit (See Figure 3 and Plate 1, panel T, at location q).

Several other sandblow pits and cones also formed during event T (see Plate 1, panel T). At least four of the six pits are located at or near the termini of major fault segments, where local shortening or extension probably was severe.

3.3.2. *Fold geometry.* Vertical deformation associated with event T is crudely represented by the isopach map of combined units 65 and 68, which were deposited in the 200-year period following the event. The fact that the structures of this isopach map (Plate 6) bear little resemblance to those of overlying unit 70 (Plate 5) is an indication that the top of unit 68 was relatively flat prior to deformation by event V. Thus the isopach map (Plate 6) is a mold of the topography that existed just after event T. However, post-T topography does not reflect event T deformation alone. Locally, broad undulations that resulted from event R were not completely mantled by post-R, pre-T units (59 and 61). Thus the post-T topography is a composite of event T deformation and preexistent topography. The existence of certain structures in the 65 and 68 isopach map (Plate 6) betrays this fact. The E-W trending contours near point "q" (Plate 6), for example, indicate that the ground surface there just prior to event T was creased by a 20-cm-deep trough trending northeastward. This trough overlies a channel in unit 59 (Plate 3, panel 7), which had been only partially filled prior to event T. Despite these complications, important aspects of event T deformation can be gleaned from Plate 6. For example, none of the larger anticlines and synclines that are prominent in event V and events X and Z have event T analogues. Several smaller event T folds are prominent, however.

At the southeast edge of the map an east trending anticline ("s," Plate 1, panel T, and Plate 6) formed during event T. This feature, which is indicative of shortening, is the sort one would expect to see in the region between two left-stepping en echelon dextral faults. About 1 m southeast of this anticline is the fissured terminus of one of the event T faults. Restoration of 1.5 m of later (event V) slippage produces alignment of the anticline and juxtaposes a small plunging syncline with the fault and fissure. Note that, as one would expect, the isopachs (Plate 6) match across the fault only where the fault did not experience appreciable slippage during event T.

3.3.3. *Lateral offsets.* Reconstruction of lateral offsets associated with event T is not as complete as the reconstruction for events X and Z. Nevertheless, several reconstructions are possible. Northwest of the center of the excavation between two major event T faults is a set of east trending folds ("r," Plates 1 and 6) from which a minimum lateral offset for event T can be inferred. These folds indicate severe shortening between en echelon fault traces. Such shortening would be an expected consequence of right-lateral slip on the two bounding faults. The minimum shortening required to produce these folds by buckling is about 70 cm, measured parallel to the faults. This value is derived by subtracting the distance A-A′ from the combined arc lengths of the undulating folded surface along cross-section A-A′ (Figure 8). This assumes that the surface simply buckled. A larger value would result if, in addition to the buckling, the folded units also thickened. The 0.7-m minimum shortening parallel to the fault translates directly into a minimum dextral offset of 0.7 m for event T.

A larger value for lateral offset during event T is recoverable about 10 m to the northwest of "r," along one of the en echelon faults. At this point, a shallow unit 59 stream channel and a unit 59 gravel pod (squares and triangles, respectively, in Plate 3, panel 7) have been offset a total of 2.0 m by event T and event V faulting. A sandblow pit at the same locality (inverted triangles in Plate 3, panel 3) has been offset about 0.8 m by event V faulting alone (discussed in section 3.2.3). Therefore about 1.2 m of dextral slip accompanied event T, here. The vertical component of the event T slip vector is about 0.5 m. This follows from two observations: First, the unit 70 isopach map (Plate 5) reveals that the vertical separation during event V ranged from 0.05 to 0.15 m, and second, the unit 59 channel cross section (Figure 9) indicates that the combined vertical offsets of events V and T is 0.6 m. The difference, 0.45–0.55 m, is the vertical component of event T slip.

A third indication of event T offset occurs along the youngest fault in the southeastern sector of the site (Figure 2 and Plate 1). Here, southeast of the event V step-over, this fault has experienced movement during events T, X, and Z but not V. The scarp and disturbances produced by event V slippage farther northwest do not appear along this segment of

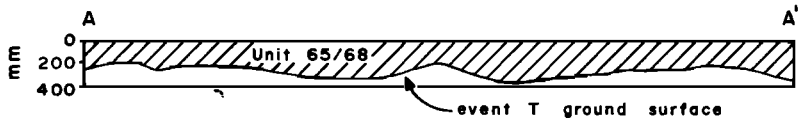

Fig. 8. A minimum of about 70 cm of dextral fault slippage during event T is indicated by these folds along cross-section A-A' in Plate 6. Horizontal and vertical scales are identical.

the fault. Various reference features (refer to discussions of X and Z above) display about 4.2 m of offset on this fault break attributable to events X plus Z. Along the same segment, the isopach map of unit 61 (Plate 3, panel 6) documents total right-lateral offsets that decrease southeastward from ~5.6 m (upright triangle in Plate 3, panels 1 and 6) to ~4.3 m (inverted triangle in Plate 3, panels 1 and 6). This indicates that along this segment, event T slip decreased southeastward from ~1.3 to ~0.1 m. This is consistent with the observation that a major left step in the event T fault zone occurs at the southeastern boundary of the map area (Plate 1, panel T).

Three offset reference features along the youngest main fault provide additional support for a combined offset of about 2.5 m for events T and V. The isopach map of unit 61 (Plate 3, panel 18) displays a thickening of unit 61 near the 14- and 21-m reference marks which probably reflects the existence of a 5-m-long east trending trough in the pre–event T surface. This trough is offset ~6.6 m along the fault. Several meters to the southeast is a broad thinning of unit 61 (not displayed in Plate 3, panel 18). This broad feature also appears in the isopach map of younger units, 65 and 68 (Plate 6). Both features reflect topography produced during event R, and both are offset the same amount: 6.8 m. (An older feature, a stringer of unit 59 gravel, appears to be offset ~7.2 m (hexagon symbols, Plate 3, panels 1 and 16). This large "offset" is not consistent with those just described and may therefore indicate about 0.4 m of nontectonic right-lateral separation rather than offset. That is, the gravel stringer may have been desposited with a 0.4-m bend across the fault.) Of the 6.6- to 6.8-m offsets along the central trace, 2.5–2.7 m is attributable solely to events T and V. In view of the 1- to 1.5-m offsets described for both T and V elsewhere in the excavation, an assumption of 1.3 m for each event on this major fault is reasonable. Thus the magnitude of right-lateral slip during T and V is about 60% of the value determined for the two later events, X and Z.

3.4. *Event R*

3.4.1. *Fault geometry.* Plate 1 (panel R) shows that the fault geometry of event R differs substantially from that of all four events described above. Principal faulting was not confined to the traces roughly bisecting the site. Instead, the prevalent event R faults constitute a zone of left-stepping en echelon fractures approximately 10 m wide. The trend of the five major traces is 10°–25° more northerly than the general northwesterly trend of the fault zone. Dips of the faults are predominantly toward the southwest, and scarps along these faults are overwhelmingly southwest facing. Thus these faults have an appreciable component of normal slip, in addition to the right-lateral slip that will be described below. Both the sense and magnitude of vertical slip across the entire zone of event R faulting are comparable to that of subsequent events V, X, and Z.

The faults of event R dip steeply westward in their upper portions. At depths below about 3 m from the event R ground surface, however, some of these faults (labeled "v" and "y" in Plate 1) are listric. The listric nature of "v" and "y" are apparent in Plate 4 and Figure 2, respectively.

3.4.2. *Fold geometry.* As one would expect for an event with such a complex system of disjunct and curving fault planes, event R produced a great deal of deformation other than faulting. Unit 59 mantles the event R surface, and an isopach map of this unit would probably provide a good mold of event R deformation. Unfortunately, construction of such a map proved too difficult because the unit has such a gradational and poorly defined lower boundary in most places that an accurate thickness is impossible to determine except locally. Unit 61, which was deposited as a thin silty peat upon unit 59, serves as a poor but useful substitute for understanding the event R deformation. The thickness of this unit appears to be inversely related to the elevation of the surface upon which is was deposited. The folds shown in panel R of Plate 1 are based on changes in thickness revealed by the isopach map of unit 61 (from which panels 6 and 18 of Plate 3 are excerpted). The isopach map reflects only some of the larger-amplitude folds because a substantial thickness of unit 59 silt and sand had already mantled the event R surface before unit 61 was laid down. It follows that the amplitude of changes in unit 61 thickness is much smaller than the amplitude of underlying event R folds.

Many of the small folds that appear in the isopach map occur in logical relationships to the faults. Small anticlines occur between left-stepping en echelon faults; synclines and anticlines occur at some fault terminations. Two local thickenings of unit 61 (Plate 1, "u" and "w") are associated with event T sandblow pits. This association probably indicates that sandblow pits formed at these localities during event R as well. Perhaps the event R pits are not directly observable because of the massive nature of the unit into which they were emplaced and because they were partially or completely reexcavated during emplacement of the event T pits.

3.4.3. *Lateral offsets.* Examination of several offset reference features indicates that event R resulted in 0.5–1 m of right-lateral slip. Consider first the offsets of a spectacular gravel-filled gully that cuts units 34–53 (Figure 10). This feature was cut and partially filled before event R, which oc-

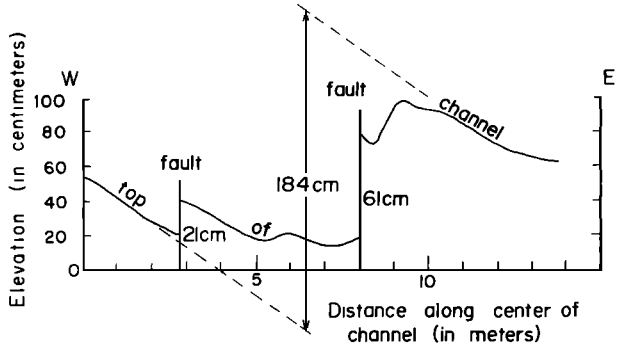

Fig. 9. Profile drawn on top of unit 59 channel sand (see map view in Plate 3, panel 7) reveals folding and fault slip associated with events T, V, X, and Z.

curred after deposition of unit 55 and before deposition of unit 59. Plate 3, panel 9 illustrates in map view its configuration at the level of unit 51. Plate 3, panel 12 depicts the gully in map view at two horizons nearer its base, at the level of units 39 and 34. The walls of the gully are highly irregular, and so horizontal exposures, closely spaced vertical exposures, and unusually detailed surveying were required to pin down the actual offset values.

Along the main recent fault, the gully is offset 7.1 m right laterally and 0.43 m vertically (Plate 3, panels 1 and 12). These values are based on the precise surveying of the southern wall of the gully at the level of unit 34. Offsets at other levels are not very well constrained along the central trace because of inappropriately wide spacing of excavations. The 7.1-m dextral offset is 0.3 m greater than that of unit 61 along the central trace (see Plate 3, panel 18 for comparison). The 0.43 m of vertical slip is about 0.1 m greater than that for unit 61. Thus, at this locality, about 0.3 m of dextral slip and 0.1 m of vertical slip occurred during event R. A few meters to the southeast, a unit 53 and 55 gravel stringer is offset only 6.9 m (Plate 3, panels 1 and 19). This may indicate that lateral slip during event R was very minor or absent along this part of this fault.

The fault labeled "v" in Plate 1, panel R, was a major agent for strike slip during event R, so the intersection of this fault and the unit 59 gully was exposed with extraordinary care. The gully crosses the fault at the major step-over in the fault that is labeled "x" on Plate 1, panel R. Thus the fault traces shown in Plate 3, panels 9 and 12, are quite complex. Figure 11 is a representative exposure of the fault and the gully.

At the level of unit 39 the northern wall of the gully is right-laterally offset a total of 0.80 m along two fault planes (Plate 3, panels 2 and 12). The southern wall is offset 0.55 m. At the level of unit 51 the southern gully wall is offset 0.50–0.60 m, and the northern wall has no appreciable lateral offset because the main fault is oriented parallel to the gully wall (Plate 3, panel 9). I conclude from these data that this fault ("x" on Plate 1, panel R) experienced 0.5–1 m of dextral offset during event R.

A similar value, though more poorly constrained, applies to this fault at "v" (Plate 1, panel R). An event I sandblow is offset between 0.3 and 1.0 m there (Plate 3, panels 2 and 8). (The figures are drawn with 1 m of offset shown, but the wide spacing between vertical exposures here allows as little as 0.3 m of offset.) Part of this offset may have occurred during event N, also.

Vertical deformation in the small region between the two en echelon traces provides a third clue as to the dextral offset during earthquake R. In this area the ground surface was warped appreciably during earthquake R. Note in Figure 11 the degree of synclinal folding of units below 59 and the relatively level repose of unit 61 above. Between earthquake R and the deposition of unit 61, unit 59 buried the warped topography. Therefore Figure 12, which is an isopach map of unit 59 in this small step-over region, presents a mold of the topography produced by event R. The originally flat ground

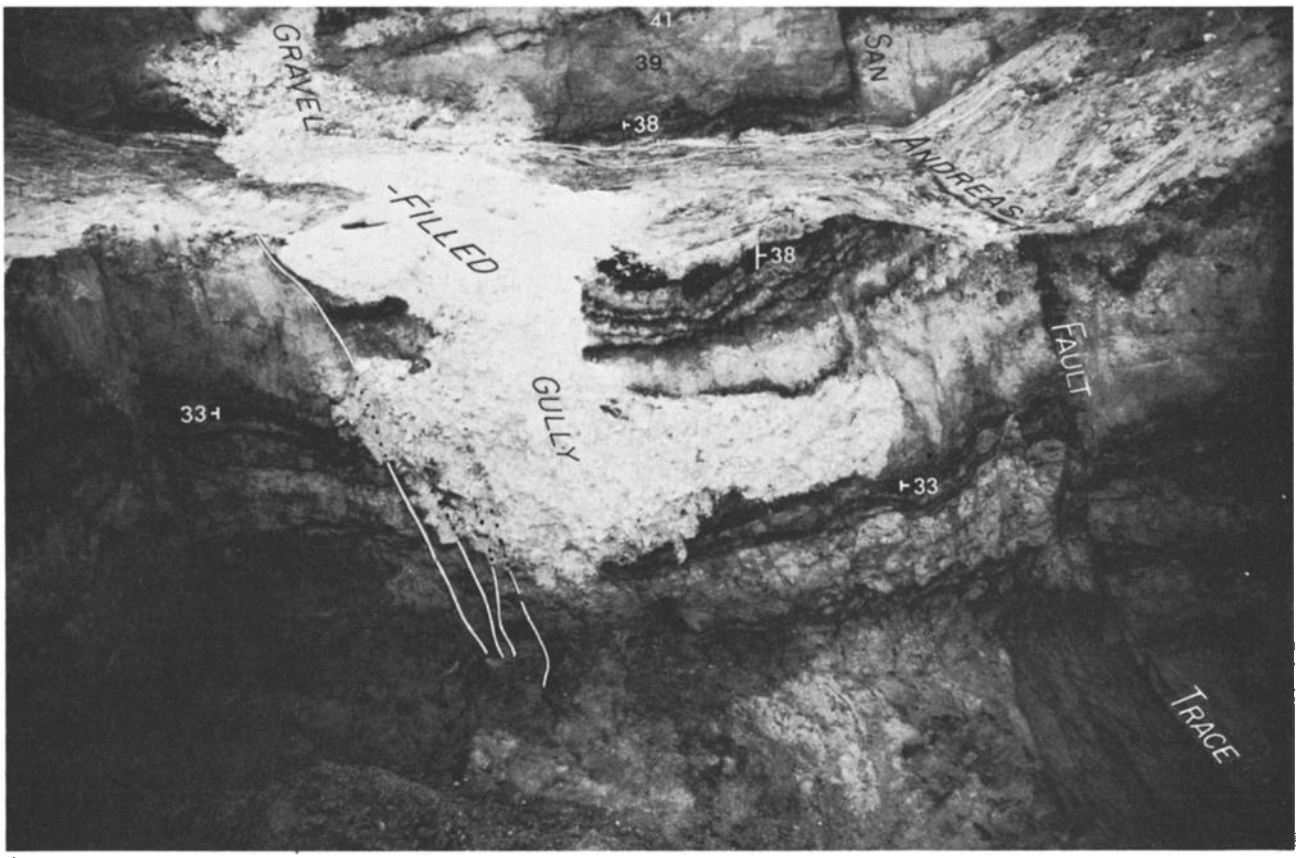

Fig. 10. Photograph of a gully that was cut into the sediments and partially filled with gravel before event R. View is southeastward. Fault on right intersects gully farther to northwest (in front of plane of paper) and offsets it 7.1 m (see Plate 3, panels 9 and 12). Fault zone on left is cut by gully and clearly antedates it. Along part of its course this gully is a subterranean pipe, eroded into units 34–50 but not breaking the ground surface that existed at the time of formation of the feature.

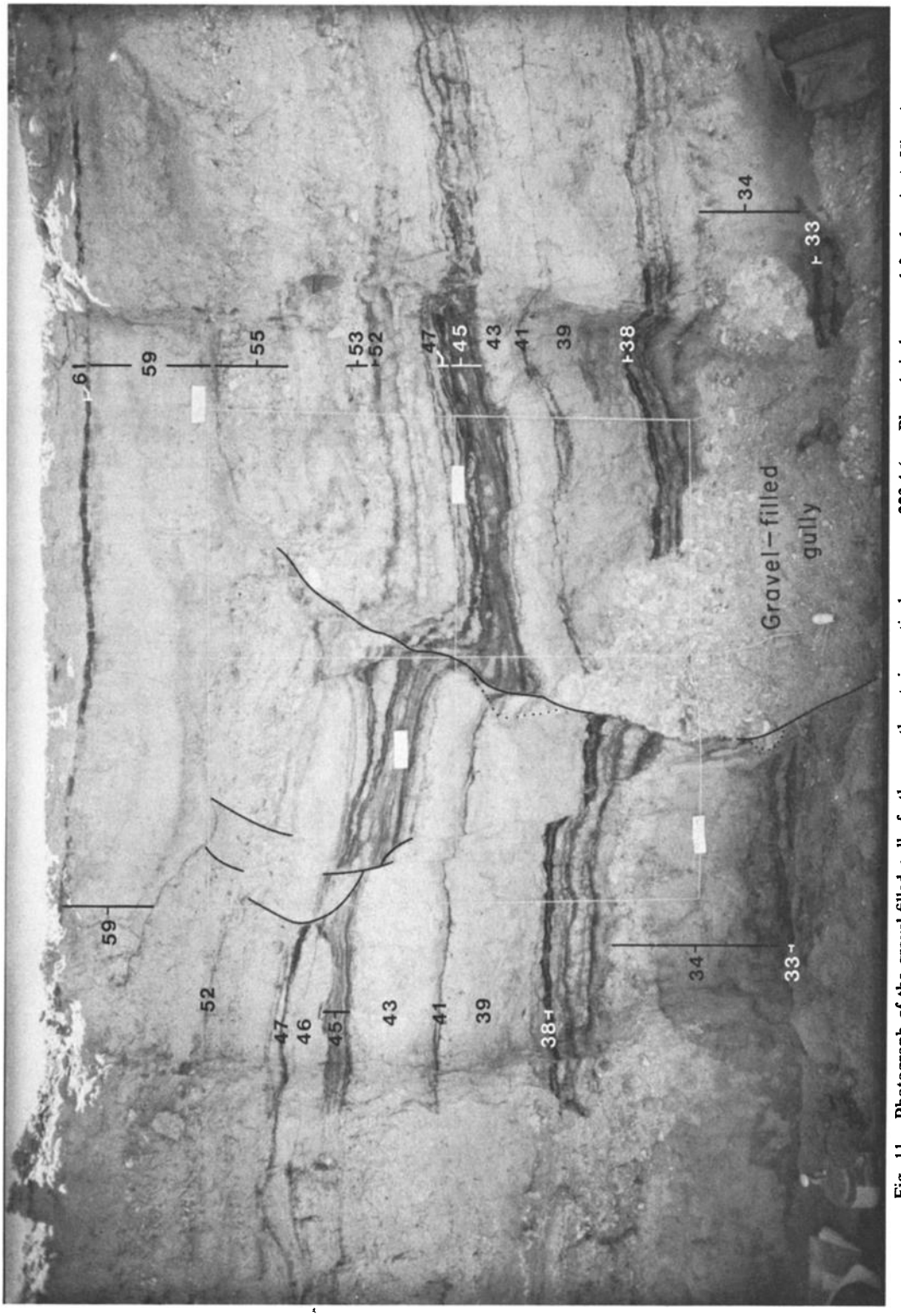

Fig. 11. Photograph of the gravel-filled gully farther southeast, in vertical exposure 223.4 (see Plate 1, index panel for location). View is southeastward. Grid is composed of 1-m squares. Notice that the gully is broken by a fault that does not break the unit 61 peat at the top of the cut. Only a small piece of the gully (outlined by dots) is visible to the left of the fault in this exposure. Eighty centimeters of dextral slip occurred on this fault during event R (see Plate 3, panels 9 and 12).

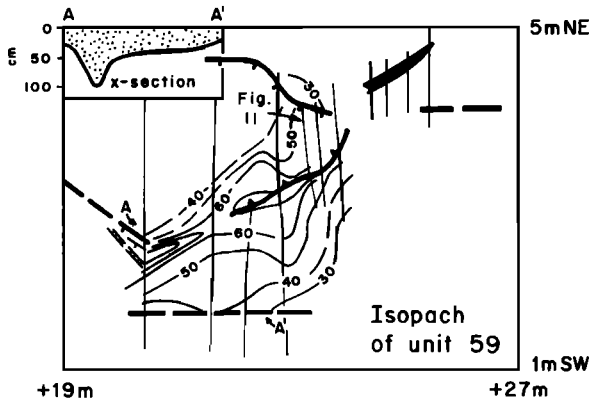

Fig. 12. Isopach map of unit 59 reveals folding and faulting of ground surface at the time of event R. Thinnest lines represent exposures used to construct map.

surface prior to R (heavy line in cross-section AA', Figure 12) must have been shortened 0.8 m to account for this much folding by buckling alone. The folding did not involve appreciable thickening of the folded units, so this value probably represents the actual shortening and not just a minimum value.

3.5. *Event N*

The occurrence of event N, between deposition of units 52 and 53, was conclusively demonstrated by *Sieh* [1978*a*, p. 3920]. Nevertheless, faults that can be associated clearly with event N are quite uncommon at the Pallett Creek site. These few faults are labeled "N" on frame R of Plate 1. Most of the en echelon faults of event R that are north of the youngest major trace (Plate 1) may also have slipped during event N. However, the stratigraphic position of the event N ground surface, just below the thick and poorly bedded gravels and sands of unit 50, hampers recognition of event N effects.

Vertical deformation produced by event N is also difficult to recognize because that part of unit 50 between the horizons of event N and event R consists of coarse, irregularly bedded sediment. Thus it would be invalid to use an isopach map of the unit as if it were a mold of N deformation.

In spite of the poor record of event N, I am fairly confident that it was not associated with major deformation or lateral offset. Analysis of several features that were deposited across the fault prior to event N suggests that the features were offset only by events that occurred after event N. For example, fault "t" (Plate 1, panel R) offsets unit 34 about 3 m and units 39 and 46 about 2.5 m. A total of 2 m is clearly ascribable to events T and V, which have been discussed above. This leaves a mere 0.5 m to be split between events N and R. The major portion of this is probably attributable to event R, which clearly ruptured this segment and had about 1 m of dextral slip on fault traces to the southeast.

Across the reverse slip fault at "x" (Plate 1, panel R), where the isopach map of unit 59 (Figure 12) revealed about 80 cm of dextral slip for event R, isopachs of units 53–55 (not presented in this report) limit the dextral offset for event N to less than 10 or 20 cm. Thus event N appears to be the youngest event at Pallett Creek not associated with dextral slip or vertical deformation similar in magnitude to that associated with the great 1857 earthquake.

3.6. *Event I*

3.6.1. *Liquefaction.* The most remarkable aspect of event I is the evidence of liquefaction preserved in the Pallett Creek record. Small sandblows, generally 1–2 m in diameter but ranging up to 10 m across, dot the event I ground surface at the site (Plate 1, panel I, and Plate 7). These sandblows, which constitute unit 46 (Figure 4), range up to 30 cm in thickness except for one large blow more than 40 cm thick at the northwest edge of the excavation. Blankets of sand less than 10 cm thick trail toward the southeast from several of the sandblows, suggesting that the ground surface at the time of event I sloped gently southeastward.

Several of the sandblows have blunt rather than tapered rims. In addition, these deposits appear to have sunk with unit 45 into the underlying sandy unit 43 and are associated with small faults that cannot be correlated between exposures and have not slipped since event I. Together, these phenomena argue for local liquefaction of unit 43, less than half a meter below the event I ground surface. Liquefied unit 43 provided poor support for the thin cap of peaty, clayey unit 45, which broke up along numerous small fractures, some of which then served as conduits for extrusion of the liquefied sand. As the sandblows were being constructed, the weight of the extruded sand depressed unit 45 into the liquefied unit 43.

3.6.2. *Fault geometry and lateral offset.* Most of the faults shown in Plate 1, panel I, are short and of small displacement and are related to the liquefaction just described. Typically, they break unit 45 but do not extend downward into units 39, 41, or 43, the sandy units that locally liquefied and were the underground sources of the event I sandblows [*Sieh*, 1978*a*]. The largest fault, however, probably represents tectonic slippage. That fault comprises two en echelon segments connected by a reverse fault. There are the same structures as those that are labeled "v" and "x" in Plate 1, panel R. Movement along the fault is suggested by an isopach map (not included, for the sake of brevity) of units directly overlying the event I ground surface. No restoration of slip along the fault enables a matching of the isopach contours across any of the fault segments. If no slip had occurred during event I, the thickness of beds deposited after event I would vary smoothly and gradually across the fault. Instead, the thickness of these beds changes abruptly at the fault, and no restoration of event N or event R slip enables a matching of the contours. This is what one would expect if the fault slipped during event I (see Figure 5 and accompanying discussion).

For the reverse fault that connects the en echelon segments, isopach data are available at very close spacing (Figure 13). The isopach pattern is compelling evidence for slippage during event I. The thick trough of sediment laying on the footwall block against the fault trace indicates that the edge of the footwall block was depressed during event I. The minimum shortening of the ground surface in the plane of the cross section in Figure 13 is given by the difference between the length of the deformed ground surface minus the length of an undeformed line across the section. That value is 10 cm. A lack of appreciable thickening of unit 45 here indicates that the actual shortening must not be more than about 15 cm.

The 10–15 cm of shortening is a direct indication of the magnitude of right-lateral slippages on the adjoining north-northwest trending fault segments. Thus it appears that event I was accompanied by merely a small fraction of a meter of right-lateral slip. This is about an order of magnitude less than the lateral slip associated with event R at the same locality within the site.

Therefore I conclude that event I, like event N, is a much smaller event at Pallett Creek than the 1857 event (Z) or events R, T, V, and X.

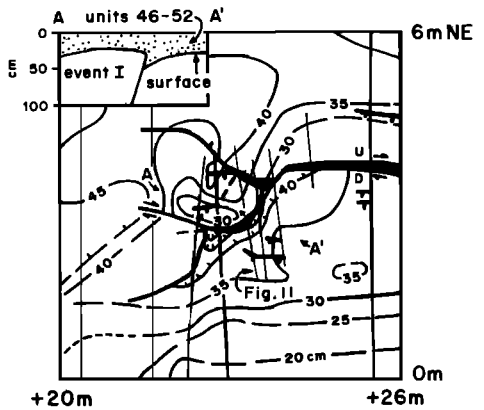

Fig. 13. Isopach map of units 46–52 reveals local folding and faulting associated with event I. Thin straight lines indicate vertical exposures used to construct map.

3.7. *Event F*

Event F is one of the more fully documented and well-understood events at Pallett Creek. The main faults of event F constitute an impressive set of southwest dipping, listric en echelon faults near the northeastern edge of the map area (Plate 1, panel F). Slip on these faults during the earthquake was oblique, with a dextral component of about 2 m and a normal component locally as great as several tens of centimeters. Evidence for vertical deformation consists of long anticlines and synclines, most of which trend obliquely to the faults. Large, elongate pits were excavated into the upper meter of sediment by pore fluid escaping rapidly during the event, after most of the fault slip had occurred.

3.7.1. *Fault geometry.* The principal fault zone of event F comprises two faults arranged en echelon, trending a few degrees more northerly than the general trend of the zone. The fault labeled "aa" in Plate 1, panel F, was reactivated during later events I, N, and R, and its trend is more oblique to the general trend of the zone at the horizons of these younger events. The trace labeled "z" in Plate 1, panel F, has not ruptured since event F. This fault, visible at the right edge of Figure 3, clearly does not rupture units deposited upon the event F horizon, unit 38.

Scarps formed along the major faults during event F face southwestward and range up to a few tens of centimeters in height. All of the major faults of event F cut units within 1.5 m of the event F ground surface at a steep angle. Curiously, however, they shallow within peaty unit 26 to dips of less than 10° (Figure 3). Farther downdip these nearly flat-laying faults steepen to dips of 60°–70° and disappear beneath the floor of the excavation. Thus these structures are tectonic and not due simply to slumping.

The reason that the faults of event F did not propagate upward through unit 26 in a more straightward manner is unclear. Perhaps the thick, fibrous, peaty unit resisted high-angle brittle fracture and tore along partings in the matted peat instead.

3.7.2. *Fold geometry.* Event F resulted in profound vertical deformation at the Pallett Creek site. This deformation consists of elongate anticlinal and synclinal folds with crest to trough amplitudes as great as 50 cm.

The isopach map of unit 39 (Plate 8) reflects these folds. Northeast of the fault zone are three anticlines and three synclines with east-west trends. Southwest of the zone of faulting is an anticline that runs roughly parallel to the fault zone throughout most of the length of the excavation.

3.7.3. *Liquefaction.* Many large sandblow pits pock the event F ground surface (Plate 1, panel F, and Plate 8). These large hollows are filled predominantly with sand from unit 39. From detailed study of several of these features we concluded previously that these pits are "sandblows," owing their origin to rapid removal of sediment by upward movement of fluidized sand [*Sieh*, 1978*a*; *Meisling*, 1980]. We argued then that the sand of unit 39 had been expelled from a liquefied layer at or beneath the base of the sandblow pit. This conclusion was wrong. Further excavation has proven that of the many pits encountered in the excavations, only one pit [*Sieh*, 1978*a*, exposure 7] is filled with sand from an underlying liquefied layer. The sand filling all other pits washed into the pits from above soon after event F. This is proven by the fact that all but one of the pits lacks a connection with underlying sandy units. Apparently, the pits formed in localities of severe deformation, where near-surface pore pressures in the water-saturated sediments became large enough to eject forceably the upper meter of sediment and thereby form the pits. Small amounts of silt and clay were deposited on the floor and walls of the pits soon after the earthquake, while the pits contained standing water. Soon thereafter, sand moving as bed load in Pallett Creek fell into and filled the pits.

3.7.4. *Lateral offsets.* Dextral offset associated with event F can be determined in two localities at the site (see arrows, Plate 1, panel F). Both of these are near the northwestern edge of the excavation. One is a well-defined sand lens within unit 38, a unit just a few centimeters below the event F ground surface (stippled pattern in Plate 3, panel 4). The lens was deposited prior to event F and well after topographic irregularities produced by the preceding event (D) had been buried. The southern edge of the sand lens is offset 2 m across the principal fault of event F. This 2-m offset must represent dextral slip during event F because no later slip occurred on this trace (see, for example, Figure 3 at "F" lower right corner).

3.7.5. *Discussion.* From the data presented above, it appears that event F is comparable in size to the great 1857 event and events R, T, V, and X. Dextral slip was 2 m along the main event F trace at one locality, and the amplitude of vertical deformation was certainly at least as great as that which accompanied events V and X and the 1857 event.

The Pallett Creek sediments also record information about the timing of event F phenomena. Relationships within the excavation show that folding occurred first, faulting occurred next, and the sandblow pits were produced last. It is clear that the sandblow pits formed after the faults had slipped because none of the pits that straddle faults are broken by event F faults. The pits 3 m southeast of "z" (Plate 1, panel F) and northwest of "aa" are particularly impressive in this regard because they straddle fault "z" and fault "aa" without being appreciably offset. The northwestern edge of the pit near "aa" was excavated centimeter by centimeter and was not found to have appreciable lateral offset. Thus the 2 m of dextral slip occurred prior to formation of these pits. On the other hand, the folds seem to have formed before the surficial fault slip occurred because isopach contours appear to be offset a meter or two across fault "z" (see Plate 8). I envision that faults propagating upward reached the base of thick, fibrous, peaty unit 26. The upward propagating fault was momentarily unable to rupture the thick, fibrous peat of unit 26. Dextral shear in the shallow subsurface was transmitted to unit 26 and overlying surficial units as a series of right-stepping en echelon

folds. As subsurface slip continued, unit 26 locally began to tear along bedding planes, and eventually faults "z" and "aa" broke the ground surface and accumulated 2 m of dextral slip. In the southeastern third of the excavation, surficial fault breaks never developed. The event F surface there consisted of folds trending obliquely across the subsurficial trace.

3.8. *Event D*

Less is known about event D than event F because the event D ground surface (unit 33) was much less extensively exposed in the excavations than was the event F surface (unit 38). Nevertheless, one can conclude from sparse exposures that the main faults of D are the same as the principal listric faults of event F (Plate 1). Event D scarps on these faults were higher than those of event F.

Isopach contours drawn for unit 34, which overlies the event D surface, indicate that an impressive set of folds also formed during the earthquake. The isopach map is not included in this report, but the folds are shown in Plate 1, panel D. The crest to trough amplitudes range up to 40 cm, about equal to the maximum values for the folds of event F. The major throughgoing anticline southwest of the fault in event F was also active during event D.

No direct measurements of dextral offset are available for this event. Nevertheless, comparable styles and magnitudes of vertical deformation strongly imply that event D and event F are similar in size.

3.9. *Older Events*

In the course of this study I have recognized three earthquakes that predate event D, which was the oldest event recognized previously. These older events are recorded in stratigraphic units not investigated in detail in my earlier study. These units, 09–33, consist of laminated, thick, fibrous peats and clayey peats interbedded with sand (Figure 4). They represent a marsh environment dominated by tall *Phragmites* grass [*Sieh*, 1977, Appendix V] and occasionally inundated by floodwaters of Pallett Creek. The sands represent the deposited bed load of those floodwaters. Peaty accumulations dominate this lower part of the section at Pallett Creek, whereas sands and gravels dominate the younger part of the section. Consideration of the causes of this difference in sedimentation is beyond the scope of this study. On both sides of the principal zone of faulting (Plate 4), the thickness of most individual sand beds is relatively uniform, indicating that the marsh surface had no appreciable relief. Several beds south of the main zone of faulting thicken toward the southwest, however, suggesting the existence of a gentle slope between the fault zone and the creek bed.

None of the units between 09 and 33 have variations in thickness which would indicate a style or magnitude of folding for the three or four earliest events that is similar to that recorded for the younger events described in preceding sections. Thus the mechanisms for folding during events D through Z, whatever it might have been, does not seem to have been operative during events A, B, or C.

Plate 4 amply reveals that structural and stratigraphic relationships within the principal zone of faulting are exceedingly complex and, in fact, largely indecipherable. This is due in part to the overprinting of faulting events D through Z on this older part of the record. Interpretation is made even more difficult by the massive and ductile nature of the peaty units and pronounced facies changes within individual peat and sand units. In addition, most of the excavations did not penetrate into units below unit 33, so evidence for events C, B, and A is limited to only a few exposures.

These complications and limited exposure preclude determination of the size or character of faulting events contemporaneous with units below 33. Nevertheless, several events can be identified and dated. Evidence for each event will now be presented, beginning with the youngest and proceeding to the oldest.

3.9.1. *Event C.* Event C is clearly recognizable in several exposures within upper unit 26. In Plate 4*a* severely disrupted fibrous peat and peaty clay is overlain by a 3-cm cap of black peat (at letter "C"). This relationship is also apparent in the opposite wall of the trench (Plate 4*b*). Several exposures near the northwestern edge of the site display listric faulting associated with event C. For example, Figure 14, which is an inset to Figure 3, shows that unit 26 is horizontally separated (A-A') by almost a meter more than unit 33 along the listric fault. Appreciable faulting occurred here during event C, just prior to deposition of uppermost 26 (solid black in Figure 14). Deposition of uppermost unit 26 and younger units through 33 then proceeded. Subsequently, these sediments were broken by faulting during events D and F.

The magnitude of event C separation along this listric fault is comparable to or perhaps greater than that experienced during event D or F. This allows a preliminary judgment that event C was a large event, comparable in size to events D and F.

3.9.2. *Event B.* Evidence for event B is recognized only in one locality. South of the main fault zone in Plate 4*a* the letter "B" indicates where the thickness of peaty units 17 and 19 has been doubled by slip along a low-angle fault. Note that thin silty beds within units 17 and 29 are duplicated across a low-angle fault. Complete lack of disruption of overlying sand beds proves that faulting took place along this structure just after unit 19 had been laid down. At first glance, the structure appears to be a thrust fault. In actuality, the contrast in thickness of subunits within units 17 and 19 near "B" cannot be explained without invoking a large component of strike slip along this low-angle structure.

3.9.3. *Event A.* The occurrence of a faulting event between deposition of units 17 and 19 is indicated in two places labeled "A" on Plate 4*a*. North of the main fault zone is a soft sediment disturbance involving units 09–17 but capped by

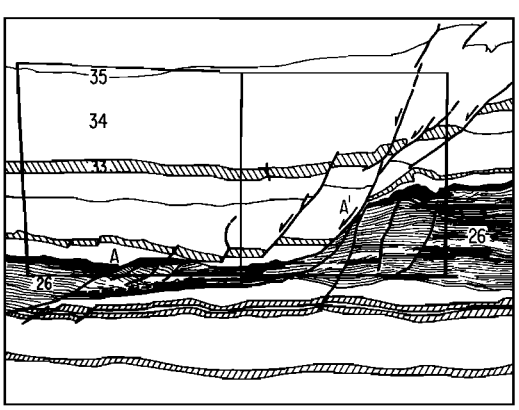

Fig. 14. Tracing from photograph of part of listric fault shown in lower right of Figure 3. Patterns and thin lines indicate peaty beds. Unpatterned areas represent sandy and gravelly beds. The squares are 1 m on each side.

TABLE 1. Radiocarbon Analyses of Samples From Pallett Creek

Sample: Pallett Creek	Sample: Laboratory	Stratigraphic Horizon	^{14}C Date $\pm 2\sigma$,[a] years B.P.	Average Date	$\delta^{13}C$ Value[b]	Isotopically Corrected Date, years B.P.	Dendrochronologically Corrected Date,[c] A.D.	Comments
							Z	
							X	
PC-2	UW-347	81	110 ± 160		(−27.4)			
PC-56B	USGS-144	81	190 ± 100	225 ± 54	(−27.4)	184	1720 to 1810 or 1645 to 1695	peat
PC-129c	USGS-897	81	250 ± 70		−27.4			
PC-102b	USGS-894	77	380 ± 90		−26.1	363	1430 to 1640	peat
PC-62	USGS-136	72	460 ± 120		(−27.4)	422	1405 to 1630	peat
							V	
PC-67	USGS-137	upper 1–2 cm of 68	320 ± 120	334 ± 66	(−27.4)	296	1485 to 1660	peat
PC-129d	USGS-895	upper 1/3 of 68	340 ± 80		−27.4			
PC-17	I-9588	upper 1/2 of 68	550 ± 160					
PC-21	I-9591	lower 1/2 of 68	515 ± 160					
							T	
PC-102c	USGS-896	upper 61	635 ± 70	658 ± 50	−25.7	647	1350 to 1390 or 1280 to 1330	peat
PC-6	UW-365	61	680 ± 70		(−25.7)			
PC-18	I-9589	61	635 ± 160					peat
PC-10	USGS-84	lower 1/2 of 61	800 ± 120		(−25.7)	789	1045 to 1295	peat
PC-222a	USGS-903	lower of two peats split off 61	1040 ± 90		−26.8	1011	940 to 1155 or 900 to 920	peat
PC-223a	UW-574	upper 50 (59?)	970 ± 100		−25.4	964	985 to 1210	charcoal, in silt
							R	
PC-28	I-9607	53	1110 ± 160					small wood and bark fragments
PC-207c	UW-573	~53 + upper 50	930 ± 100		(−25.0)	930	995 to 1220	charcoal (reburned for $\delta^{13}C$ to CO_2 from CH_4 suspect)
							N	
PC-207b	USGS-904	52	1190 ± 80		−26.9	1160	720 to 710 or 770 to 980	peat
PC-27	I-9606	51	835 ± 180					charcoal
PC-12	USGS-83	49	1130 ± 90		(−27.0)	1098	780 to 1020	peat
PC-11	USGS-82	47	1020 ± 100		(−27.0)	988	905 to 920 or 980 to 1185	peat
PC-29	I-9608	47	585 ± 160					peat
							I	
PC-64	USGS-138	upper 1 cm of 45	1130 ± 130		(−27.0)	1098	720 to 730 or 770 to 1035 or 1140 to 1145	peat
PC-5	UW-349	upper 43	1285 ± 170		(−25.0)	1285	580 to 980	Pinus (lambertiana?) wood from large trunk or branch
PC-26	I-9605	lower 43	1480 ± 160					small wood fragments
PC-25	I-9592	lower 43	1680 ± 160					small wood fragments
PC-61	USGS-139	41	1160 ± 120		(−27.0)	1128	695 to 690 or 720 to 745 or 770 to 1220	peat
							F	
PC-14	UW-379	38	1050 ± 80		(−27.0)	1018	900 to 1150	peat
PC-19	I-9590	38	1075 ± 160					peat
PC-42	USGS-141	36	1460 ± 120		(−27.0)	1428	435 to 705	peat
							D	

PC-57	USGS-140	upper 33	1410 ± 100		(−27.0)	1378	560 to 715 or 730 to 750	peaty clay
PC-414g	USGS-901	31S	1370 ± 100		−27.1	1336	600 to 775	peat
PC-414f	USGS-902	upper 3 cm of 26S	1385 ± 70		−27.1	1351	750 to 770 or 610 to 715 C	peat
PC-415a peat	A-2150	upper 6 cm of 26N	1565 ± 140		−27.6	1521 ± 43	420 to 640	peat
PC-415a cell	A-2153	upper 6 cm of 26N	1530 ± 110		−25.7			peat cellulose
PC-59	USGS-142	~mid-26N	1830 ± 100		(−27.0)	1798	70 to 380	peat
PC-415b peat	A-2151	upper 5–6 cm 19N	1670 ± 130		−27.0	1648 ± 48	260 to 535	peat
PC-415b cell	A-2154	upper 5–6 cm 19N	1720 ± 140		−28.8			peat cellulose
PC-414d	USGS-899	upper 5 cm 19S	1870 ± 70		−27.4	1832	300 to 320 or 70 to 270 A	peat
PC-414j	USGS-898	upper 4 cm 17N	1940 ± 80		−27.9	1894	20 to 225	peat
PC-415c peat	A-2152	09N	1690 ± 130		−27.9	1644	230 to 565	peat
PC-415c cell	A-2155	09N	1950 ± 290		−27.1	1916	−312[d] to 425	peat cellulose
PC-414a	USGS-900	lower 2 cm 09S	1980 ± 90		−28.2	1929	0 to 220	peaty silty clay
PC-4	UW-348	4 m below terr top	1860 ± 180	1933 ± 106	(21.14)	1995	−185[d] to 130	cedar or juniper branch (~8-cm diameter)
PC-4 wood	UW-547	4 m below terr top	1970 ± 130		−21.14			cedar or juniper branch (~8-cm diameter)
PC-4 cell	UW-548	4 m below terr top	1670 ± 110		−20.14	1748	130 to 420	wood cellulose

[a]The dates reported by the laboratories. Dates from one of the laboratories (I samples) listed were not utilized because several of the dates are quite inconsistent with the results of the other four laboratories. In cases where a horizon is represented by more than one age determination the dates have been averaged, as suggested by *Long and Rippeteau* [1974].

[b]Values for $\delta^{13}C$ are reported for some samples analyzed after 1977. The ^{13}C analyses enable reported ^{14}C ages of these samples to be corrected to include effects of isotopic fractionation between the atmosphere and the plant when it is alive and metabolizing [*Broecker and Olson*, 1959, 1961]. The corrections range from 0 to 80 years. Each sample for which $\delta^{13}C$ values were not determined has been corrected using an assumed $\delta^{13}C$ value which is indicated by parentheses.

[c]Isotopically corrected ^{14}C ages do not represent real ages because they are based on an assumption that the concentration of atmospheric ^{14}C has not varied with time. Carbon 14 dating of tree rings of known age has demonstrated that this assumption is not valid. The real (or calendar) age of the isotopically corrected ^{14}C ages have been determined using the dendrochronological calibrations of *Stuiver* [1982]. For example, PC-6 and PC-102C yield an isotopically corrected ^{14}C age of 647 ± 50 years B.P. for unit 61. According to *Stuiver* [1982] a sample with this range of radiocarbon ages formed between 1280 and 1330 A.D. or between 1350 and 1390 A.D.

[d]Minus 2σ limit from *Damon et al.* [1972].

unit 19. South of the main fault zone is a zone of complex deformation and facies variation in units 09–17 which is also capped by 19. In both localities the deformation could be related to more than one episode of faulting between deposition of units 17 and 19, but structural and facies complexities preclude differentiation of more than one event. At this time one can only say that at least one disruption occurred after deposition of unit 17 and before deposition of unit 19.

4. TIMING OF THE EARTHQUAKES

Radiocarbon dates for many peat-, charcoal-, or wood-rich strata within the Pallett Creek section provide the geochronological framework upon which the dates of the earthquakes are based. Table 1 presents and explains all of the radiocarbon analyses made on samples from Pallett Creek. These 46 analyses represent 24 horizons within the section. Sample ages not reported previously include those 19 which have Pallett Creek (PC) sample numbers greater than 100.

This suite of dates provides a chronological framework within which the date of each earthquake can be placed. The most straightforward manner of doing this is to average the dates of beds that directly overlie and underlie the earthquake horizon (e.g., events V, R, I, F, D, and C). However, some earthquake horizons are not so tightly bracketed by dated strata, so the earthquake date must be estimated from the date of a directly underlying or overlying bed alone (e.g., events X, T, N, B, and A). Table 2 lists the earthquake dates derived in this way.

The dates thus derived for the latest five earthquakes are stratigraphically consistent, and I adopt them as the best estimates that can be calculated with this set of data. However, the dates of several earlier events are not well constrained using this method. Note that the dates of events F, I, and N are indistinguishable or, perhaps, even chronologically inverted, as are the dates of events C and D.

Estimates of dates for events A through N can be improved by combining stratigraphic information with the radiocarbon analyses. From their relative stratigraphic positions we know that event A occurred prior to B, B occurred prior to C, C occurred prior to D, and so on. Each pair of earthquake horizons are separated by beds of clay, silt, peat, and/or gravel. If one estimates the time required to deposit these intervening strata, one has estimated the time between earthquakes. The sand and gravel beds are fluvial, and I have assumed that each was deposited very rapidly. The clays, silts, and peats are quiet water, aeolian, and biogenic deposits and must represent most of the time during which the section was accumulating, unless major unconformities have not been recognized. The only major unconformities recognized within the entire section are at the top (~1910 A.D. to present), between units 68 and 65 (~1350 to ~1500 A.D.), and between units 55 and 59 (~1100 A.D.). No horizons below unit 55 contain sedimentological evidence of a long hiatus in deposition (i.e., burrow concentrations, stone lines due to bioturbation, lag gravels due to aeolian deflation, or other erosive contacts).

Figure 15 shows each radiocarbon date plotted with respect

TABLE 2. Estimated Dates of Latest 12 Earthquakes at Pallett Creek

Event	Date,[a] A.D.	Remarks
Z	1857	Historically documented.
X	1720 ± 50	Unit 81 date is within period from 140 to 305 years B.P.[b] (i.e., 1730 ± 80 A.D.); event occurs at top of unit, so ~20 years must be added to unit 81 date[c], thus 1750 ± 80 A.D.; historical record precludes event after 1769, thus 1720 ± 50 A.D.
V	1550 ± 70	Weighted average of upper unit 68 (1405–1630 = 1518 ± 112 A.D.) and unit 72 (1485–1660 = 1573 ± 88 A.D.), which bracket the earthquake horizon.
T	1350 ± 50	Unit 61 date is within period from 1280 to 1380 (i.e., 1330 ± 50 A.D.); event occurs at top of unit, so ~20 years must be added to unit 61 date, thus 1350 ± 50 A.D.
R	1080 ± 65	Weighted average of samples PC-223a, PC-28, and PC-207c, which bracket the earthquake horizon.
N	870 ± 130	Unit 52 date is within period from 720 to 980 A.D. (i.e., 850 ± 130 A.D.); event occurs at top of unit, so ~20 years must be added to unit 52 date[c], thus 870 ± 130 A.D.
I	1010 ± 115	Weighted average of unit 47 (905–1185 = 1045 ± 140 A.D.) and unit 45 (710–1145 = 930 ± 210 A.D.), which bracket the earthquake horizon.
F	1015 ± 115	Weighted average of unit 41 (695–1220 = 960 ± 265 A.D.) and unit 38 (900–1150 = 1025 ± 125 A.D.), which bracket the earthquake horizon.
D	630 ± 80	Weighted average of unit 36 (435–705 = 570 ± 135 A.D.) and unit 33 (560–750 = 655 ± 95 A.D.), which bracket the earthquake horizon.
C	640 ± 65	Average of two dates for upper unit 26 is 640 ± 65 A.D. Earthquake horizon is within this unit.
B	305 ± 95	Average of 2 dates for upper unit 19 is 305 ± 95 A.D. Earthquake horizon is capped by this unit.
A	135 ± 105	Upper unit 17 date is within period from 20 to 225 A.D. (125 ± 105 A.D.). Event occurs at top of unit, so add 10 years[c].

[a]Rounded to nearest 5 years; error limits are about 95% confidence level.
[b]B.P. is Before Present. Present is defined as 1950 A.D.
[c]See *Sieh* [1978*a*, pp. 3932–3933].

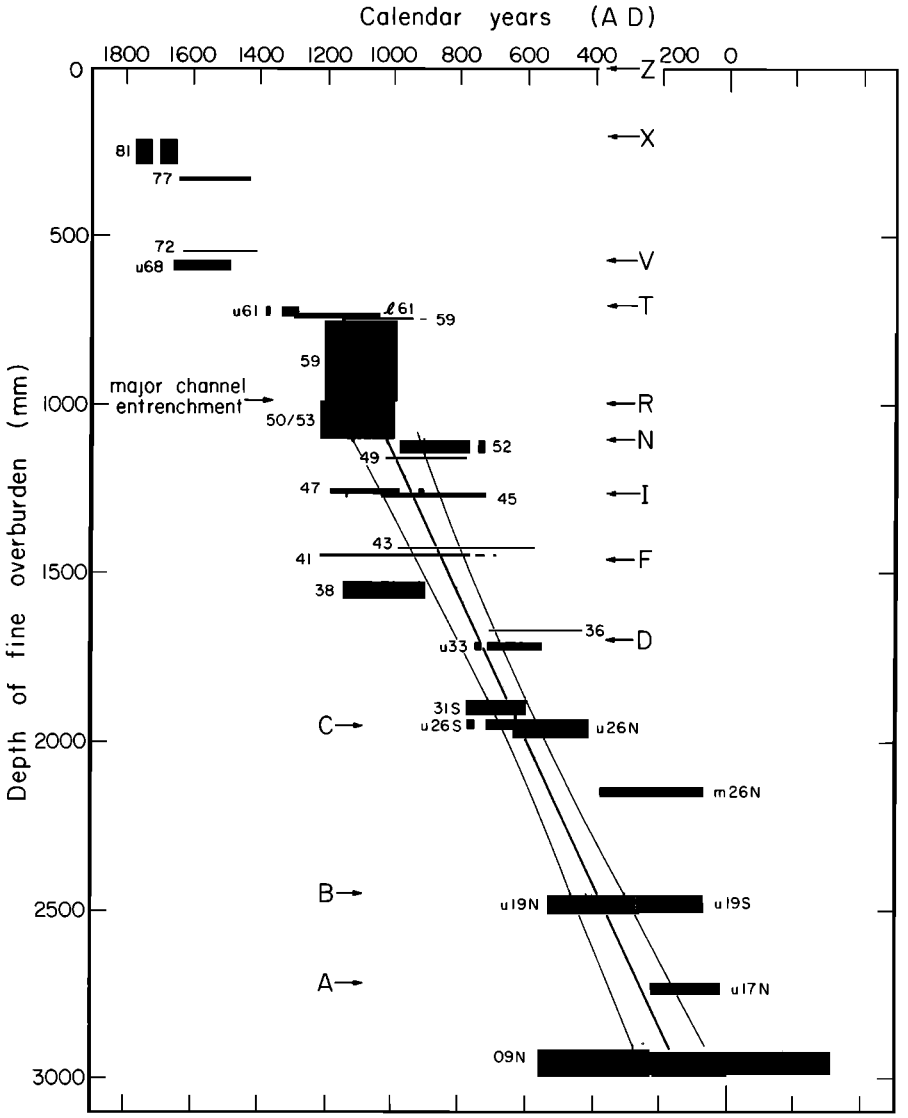

Fig. 15. Corrected ages of the individual samples plotted against their average depth beneath the ground surface. The thickness of coarse deposits have not been included. See Table 1 for radiocarbon data in tabular form. Regression line through dates of units 09–59 enables estimate of dates of events A through R.

to its stratigraphic depth. Coarse fluvial debris has been excluded from the section because it was probably deposited much more rapidly than the clays, silts, and peats. The depth of each stratigraphic unit was determined by averaging many individual, vertical columns taken from trench 11 of *Sieh* [1978*a*] and the exposure shown in Plate 4*a*.

Assuming that sedimentation rates of the fine-grained deposits are uniform and that no hiatuses are more than a decade or two long, the least squares regression against the dates of units 09–50/53 (described by D. R. Brillinger et al., manuscript in preparation, 1984) provides an estimate of the dates of events A through N. The date of each event can be read directly from the regression line which is bounded by lines showing $\pm 2\sigma$ error limits. The dates of events A through N determined in this fashion are listed in Table 3.

Combining the stratigraphic and radiometric data in this way insures that no earthquake dates will be chronologically inverted and recognizes that stratigraphically reasonable separations between events must be maintained. It is also superior to using only the radiometric dates because each earthquake date is controlled by more than just those few dates from nearby strata. This reduces the opportunity for a sampling or laboratory blunder to grossly affect the estimated date of an earthquake. The assigned error limits for events A through N actually are at less than a $\pm 2\sigma$ (95%) confidence level because uniform sedimentation rates and continual sedimentation has been assumed in these estimates. Nevertheless, I believe these to be the best estimates for the dates of events A through N.

TABLE 3. Estimated Dates of Earthquakes A Through N, Using Alternate Method

Event	Date, A.D.
N	1015 ± 100
I	935 ± 85
F	845 ± 75
D	735 ± 60
C	590 ± 55
B	350 ± 80
A	260 ± 90

5. DISCUSSION AND CONCLUSIONS

In the preceding pages I have presented data which enable better constraints to be placed on the dates and sizes of large earthquakes recorded at Pallett Creek. How can these observations now be interpreted in terms of the past and future behavior of the San Andreas fault in southern California?

5.1. *Anomalously Low Slip Rate at Pallett Creek*

Taken together, the major faults exposed at the Pallett Creek site accumulated about 10 m of slip between about 735 and 1857 A.D. This yields an average slip rate of only 9 mm/yr, a value that is only one third to one fourth of Holocene slip rates determined elsewhere along the San Andreas fault [*Sieh and Jahns*, 1984; R. J. Weldon and K. Sieh, unpublished manuscript, 1984]. Likewise, the offset attributed to the 1857 earthquake at the site is a mere 2 m, whereas 3–4.5 m have been attributed to this event on the basis of offset stream channels nearby [*Sieh*, 1978*b*].

To explain these unexpected discrepancies, one cannot call upon unexcavated major traces because this possibility has been ruled out (see discussion of Figure 1 above). It is reasonable to hypothesize that the Northern Nadeau fault, a short, discontinuous, secondary, late Holocene structure (Figure 1), is contributing a millimeter or two per year. In addition, the collection of minor faults within the excavation may reasonably be allowed a couple of milliimeters per year. The most prominent example of this is the minor fault in Plate 3, panel 19, which experienced 1.5 m of right-lateral slip between 1000 and 1857 A.D. Thus this fault contributed about 2 mm/yr of slip for the period 1000–1857 A. D. Several secondary faults and fissures in the northwestern and southeastern sectors of the site could have experienced a few tens of centimeters of strike slip during events V, X, and Z (Plate 1, panel X and Z and panel V). This much slip would not be readily apparent in the isopach and structure contour maps (Plates 2 and 5) used to determine the larger offsets because the spacing of the excavations used to make these maps was generally 1–2 m across these secondary features. One could hypothesize, for example, 25 cm of slip on the monocline between "a" and "b" or the secondary fissure and fault near "f" and "g" (Plate 1, panel X and Z) during events X or Z. This would yield a slip rate for the period 1550–1857 A. D. nearly a mm/yr greater than that determined using only the offset across the main trace. Nonbrittle buckling of the Pallett Creek sediments within the limits of the site could be evidence for additional strike slip in amounts similar to that hypothesized above for secondary faulting. The gentle folds associated with events D, F, R, V, X, and Z, for example, might represent surficial buckling resulting from distributed subjacent strike-slip shear. For each event the amplitudes of the associated folds are small and are consistent with right-lateral shear displacement of 10–20 cm. This could contribute an additional millimeter or two per year to the slip rate.

Minor faulting and nonbrittle folding within the site and slip on the Northern Nadeau fault can probably account for no more than several millimeters per year of the 15 or 25 mm/yr discrepancy. Explanations for the discrepancy of remaining 10–20 mm/yr remain elusive. Regional warp outside the limits of this site seems to be the only plausible mechanism remaining. Such an explanation would not be entirely ad hoc, since the Pallett Creek site is located very near a major 300 m left step in the fault trace, and strike-slip offset might be expected to be appreciably less on the major traces near the stepover.

Taken together, minor faulting and warping at the latitude of the site could conceivably provide the additional 15–25 mm/yr of right-lateral slip that would be required to bring the slip rate up to the levels documented at sites to the northwest and southeast. However, further investigation is clearly needed to account adequately for this discrepancy.

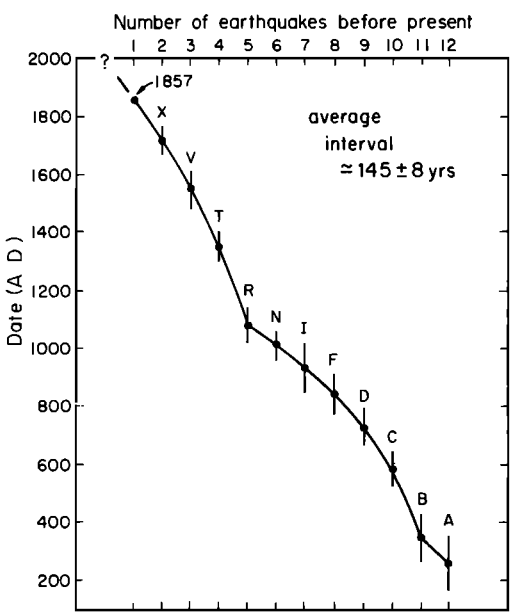

Fig. 16. Revised dates of each earthquake at Pallett Creek. See Tables 2 and 3 for listing of dates.

5.2. *Average Recurrence Interval*

Various ambiguities preclude a unique interpretation of the Pallett Creek data with respect to earthquake recurrence interval. Reasonable interpretations of the Pallett Creek record constrain the average recurrence interval for large events to be between about 145 and 200 years. The several plausible hypotheses that provide this range of values merit the following discussion.

The average recurrence interval between the 12 latest earthquakes identified at Pallett Creek is 145 ± 8 years (Figure 16). This value is derived simply by subtracting the date of the earliest event, A (261 ± 91 A.D.), from the latest event, Z (1857 A.D.), and dividing by the number of intervals (11). This value is 19 years less than was calculated by *Sieh* [1978*a*] from a smaller set of data. The error limit of 8 years is merely the uncertainty in the value of the average. It is not an expression of the range of individual values about the mean. Individual intervals, in fact, seem to span a range from about a half to about two and a half centuries.

The average interval of 145 years would represent the average interval for large earthquakes only if all the events seen at Pallett Creek were large and if all large seismic events are indeed discernable in the stratigraphic record there. These two possibilities need to be discussed. On the basis of measured lateral offsets we can be confident that the latest five events (Z, X, V, T, and R) and event F represent large earthquakes. Events D, C, and B are probably large, also. The small offsets associated with events I and N raise doubts that these two events were large, although one can hypothesize that I and N represent large events whose breaks ended in the proximity of Pallett Creek.

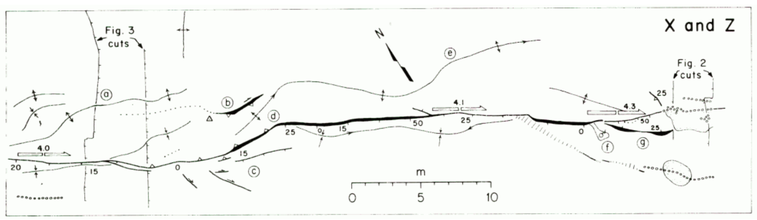

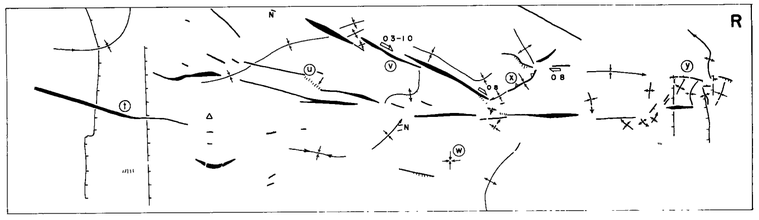

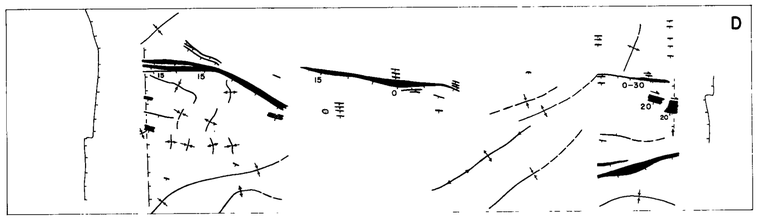

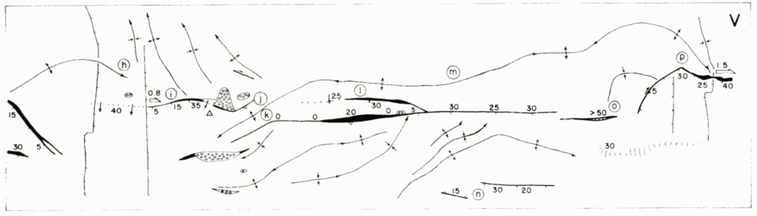

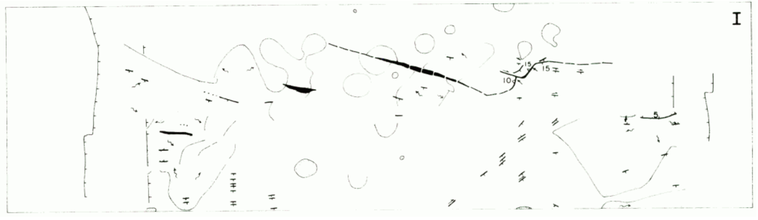

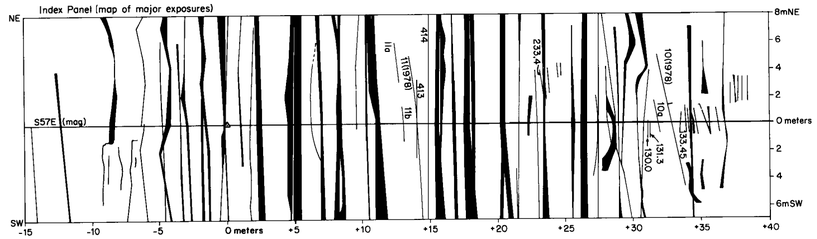

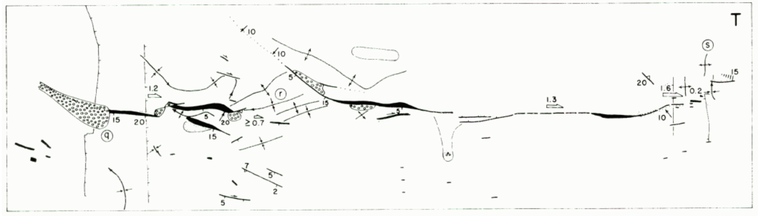

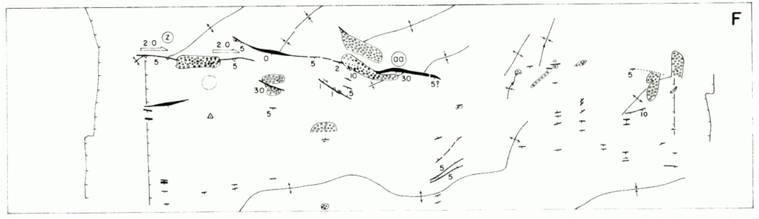

dashed where uncertain;
dotted where buried;
triangle indicates reverse separation;
Fault trace: hachure indicates normal separation;
arrow indicates dextral slip,
number indicates scarp height (in cm),
small dots indicate trace of major fault in later events

Strike slip during event in meters (segmented in panel XZ to show individual contributions of X and Z)

Open fissure (with depth in cm).

Sandblow (open circles indicate pit or fissure below surface; dots indicate cone or wedge on surface; for event I, edge of blow is 10 cm contour.

Flow direction of sandblow material.

Folds

Monocline with fault in subsurface (amplitude in cm).

Spring.

Exposures of Figures 2 and 3; hachures on side of cut.

Plate 1. Summary maps of fault breaks, fissures, sandblows, folds, and other phenomena associated with individual earthquakes. Features of each event are shown relative to the same 15 × 55 m rectangle, and location of exposures shown in Figures 2 and 3 are also shown for reference on each frame. Map above legend shows location of all major exposures used to construct these maps, instrument station (triangle with dot), and baseline trending S57°E (magnetic) through the cut. Thick solid lines indicate dipping cuts. As many as four separate levels of cut are superimposed in this index panel. Numbers identify cuts specifically mentioned in text or by *Sieh* [1978*a*]. The panel labeled "X and Z" displays faults, fissures, folds and sandblows associated with events X and Z. Likewise, the other maps portray the faulting and other phenomena associated with events V, T, R, I, F, and D. Lowercase letters in the panels identify localities discussed specifically in text. Each feature shown is mapped as its "trace" appears on the unit that was the ground surface at the time of the specific earthquake. Deformation resulting from later events has not been subtracted because of the uncertainties in any such reconstructions. For example, features below (southeast of) the main fault in the map of event V were shifted during later evnets X and Z about 4 m to the left in relation to features above (northeast of) the main fault. This has not been subtracted in constructing the diagram of event V faulting.

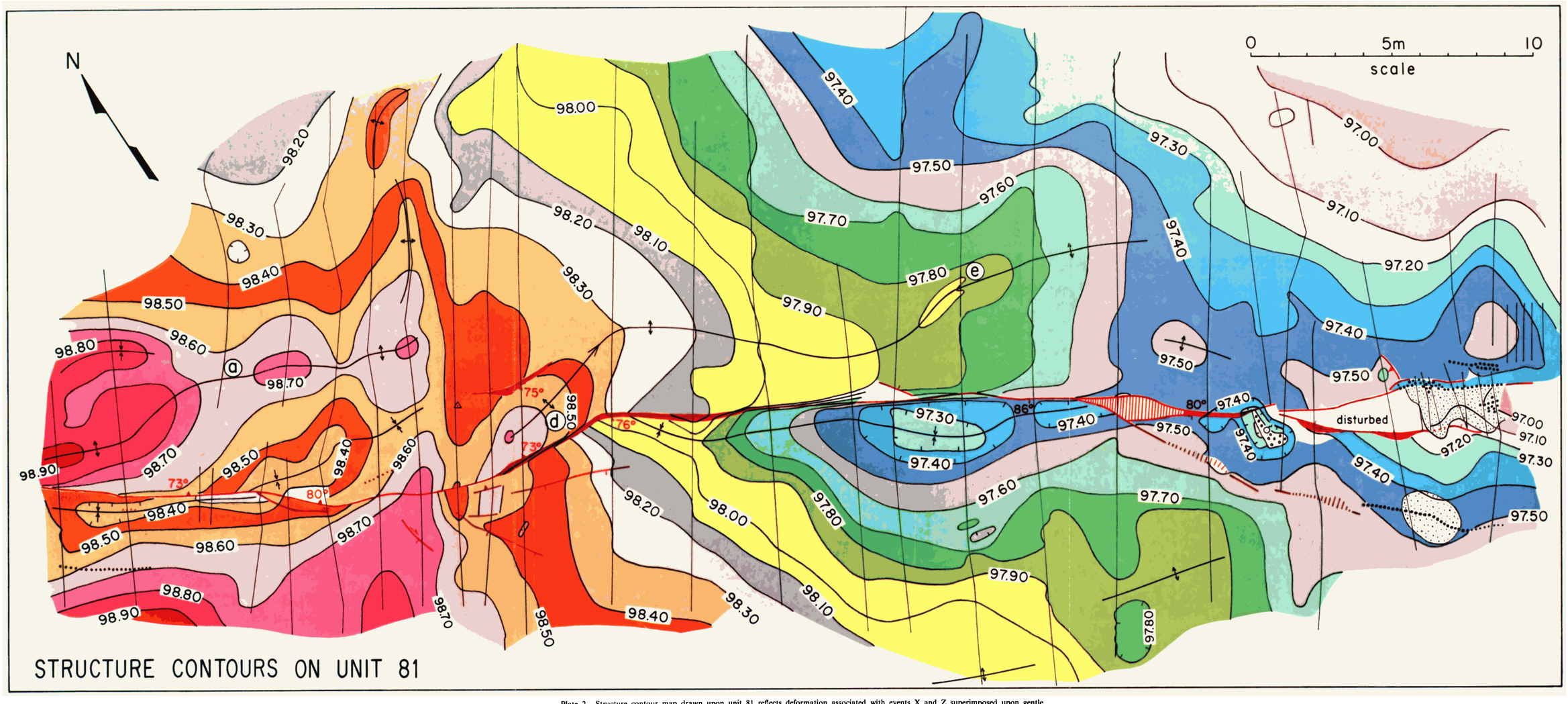

Plate 2. Structure contour map drawn upon unit 81 reflects deformation associated with events X and Z superimposed upon gentle southeastward topographic gradient. Contour interval is 10 cm. Datum of 100 m was chosen arbitrarily. Folds inferred from the structure contour map, faults, fissures, sandblows, and springs are also plotted. Symbols are as in Plate 1. Thin lines indicate excavations used as basis for this map.

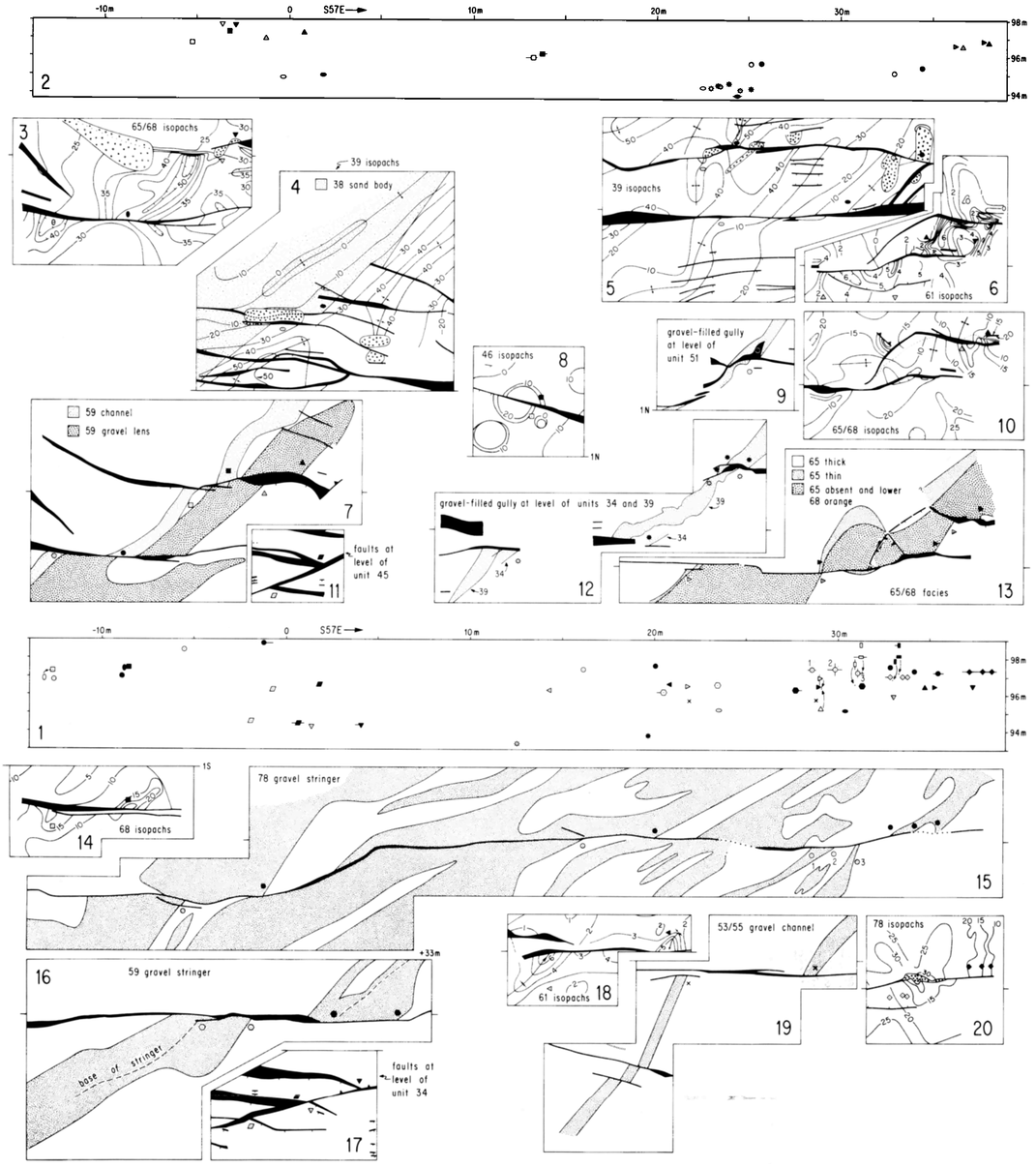

Plate 3. Maps (panels 3–20) and vertical sections (panels 1 and 2) showing right-lateral offsets recorded in the sediments of Pallett Creek. Top and bottom edges of panels 3–20 trend S57°E, parallel to the fault. Offset features are displayed as offset piercing points in the vertical planes represented by panels 1 and 2. These panels also trend S57°E, parallel to the fault. Features trending into a fault from the side of the reader are shown as open symbols. Features trending into the fault from the side opposite the reader (east) are shown as solid symbols. Offsets along most recently active major fault (i.e., principal fault of events X and Z) are plotted in panel 1; offsets along older, more northern faults are plotted in panel 2. Markings at top of panels 1 and 2 follow the surveying convention shown in the index panel of Plate 1. All maps and vertical sections have identical scale. Left-to-right placement of all plan view maps except box 16 are consistent with these markings on panels 1 and 2. For example, circled dot and solid circle at the far left of panel 1 (about −13 and −9 m) represent the offset unit 59 channel marked by the same symbols in panel 7 directly above. Open and solid squares at about −5 and −3 m in panels 2 and 7 represent the same channel, offset along a more northern fault. The NE-SW position of each plan view map is indicated by the small tick marks on the left and right edge of each panel. Unless otherwise noted, these ticks indicate the intersection of the panel with panel 1, which is directly below the surveyed baseline ("0" in index panel, Plate 1). Markings on right edge of panels 1 and 2 indicate elevation relative to arbitrary datum of 100 m. Only well-constrained offsets are indicated by the symbols. Where location of a piercing point is more uncertain than the size of the symbol, horizontal and vertical bars attached to the symbol in panel 1 or 2 indicate amount of uncertainty.

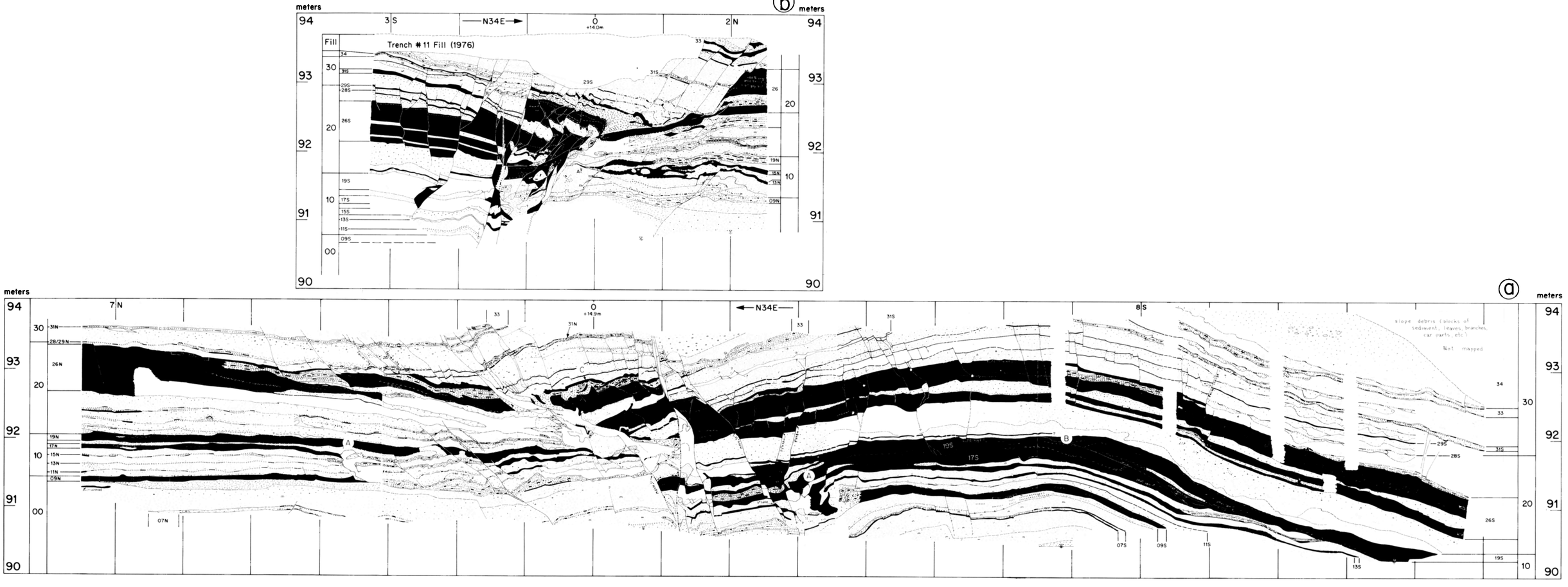

Plate 4. Detailed trench logs of units 09–33 reveal evidence for events A, B, and C, three previously unknown earthquakes at Pallett Creek. (*a*) Southeast wall of trench, labeled 414 in Plate 1, index panel. (*b*) Northwest wall of trench, labeled 413 in Plate 1, index panel.

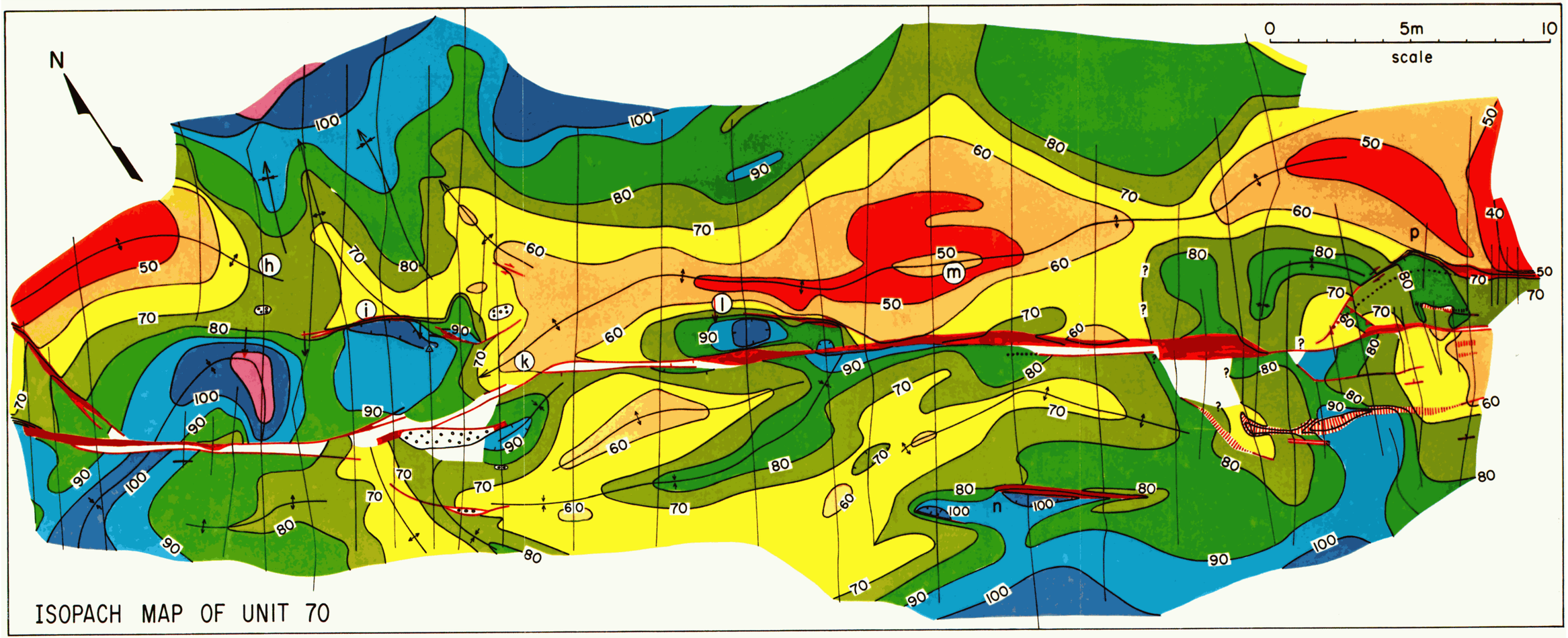

Plate 5. Isopach map of unit 70 is a mold of deformation produced during event V. Contour interval is 10 cm. Event V fissures, event V folds inferred from the isopach map, and faults cutting unit 68 are also plotted. Symbols are as in Plate 1. Note that pattern of faults shown here differs from the pattern shown in Plate 1, panel V. This figure shows all faults which break the event V ground surface (that is, event V, X, and Z faults). Plate 3, panel V, displays only those faults which slipped during event V.

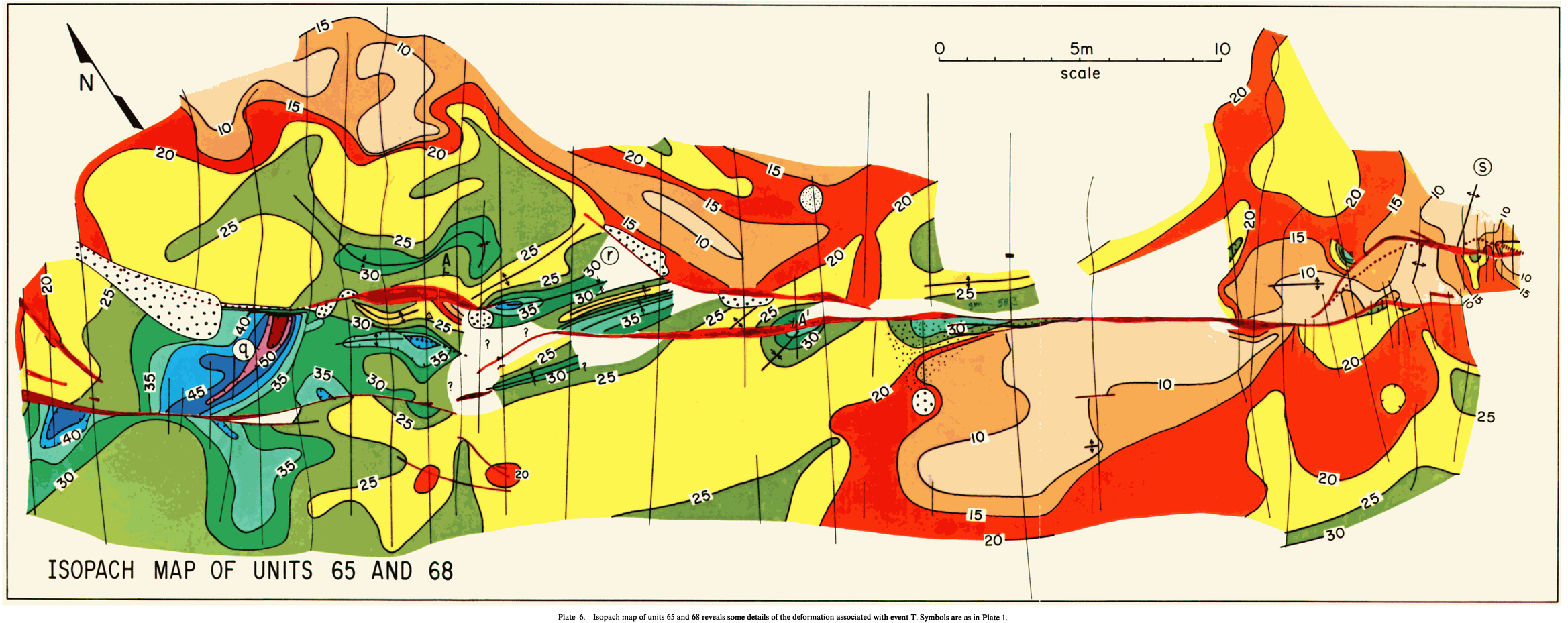

Plate 6. Isopach map of units 65 and 68 reveals some details of the deformation associated with event T. Symbols are as in Plate 1.

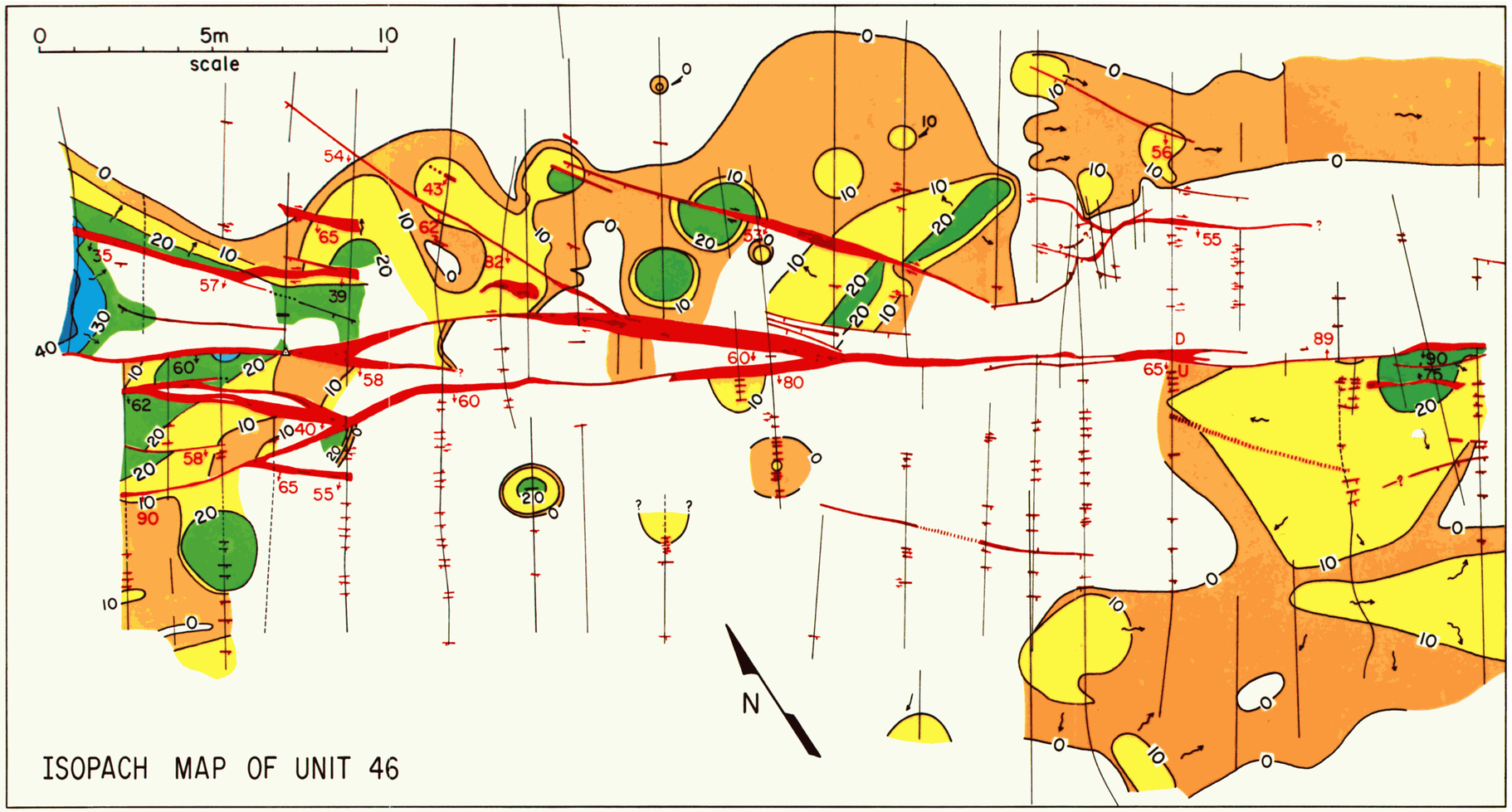

Plate 7. Isopach map of unit 46 displays the arrangement of sandblow deposits on the ground surface after event I. Thinnest lines indicate exposures used to construct map.

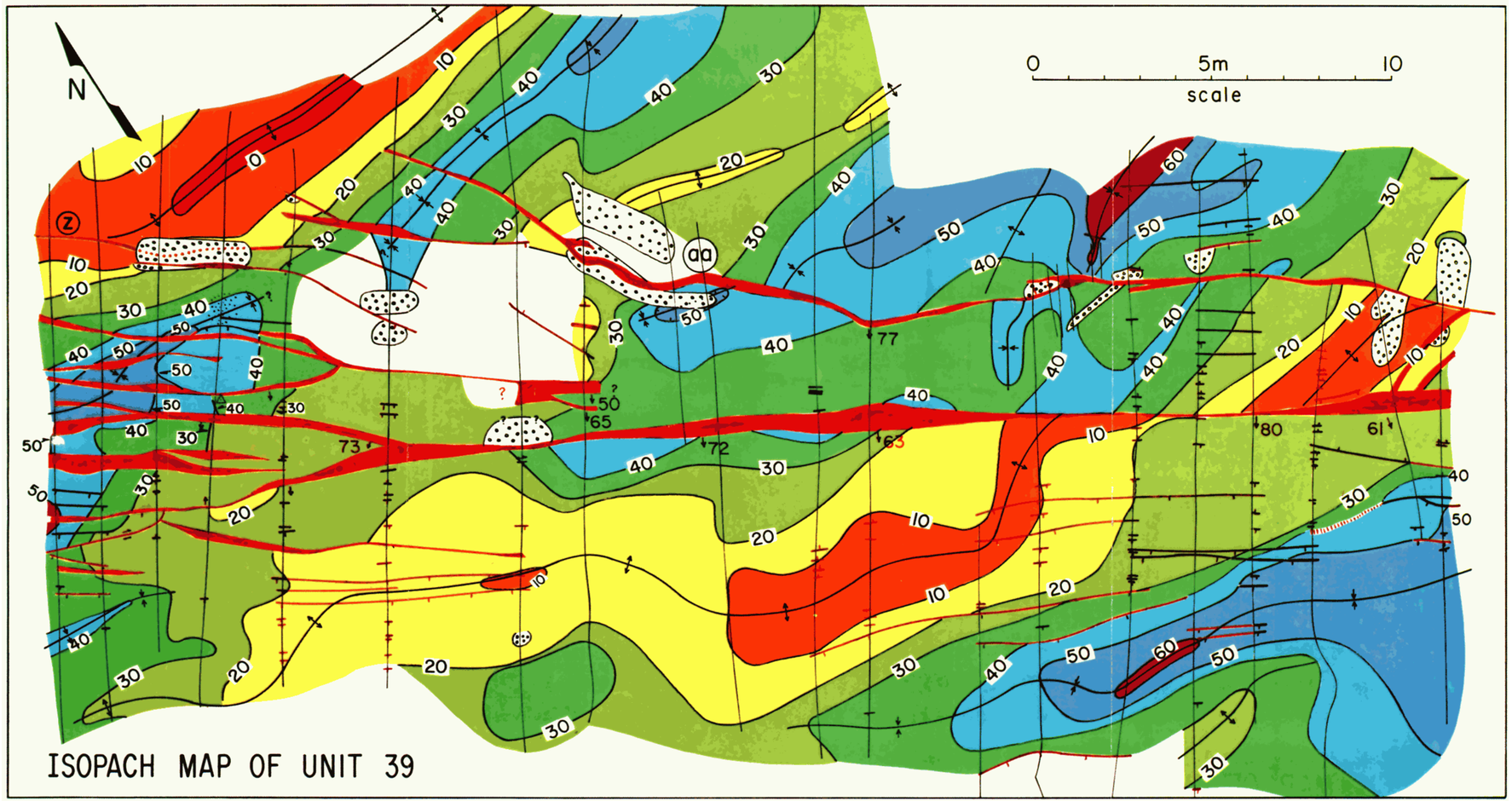

Plate 8. Isopach map of unit 39 is a mold of surficial deformation related to event F. Event F sandblow pits, event F folds inferred from the isopach map, and faults cutting unit 38 are also plotted.

The most cautious estimate of average recurrence for large earthquakes would use only the latest five events. The interval between these events averages 194 ± 16 years. Hypothesizing that I and N are small and utilizing large event F, an average of 203 ± 15 years is obtained for the period 845–1857 A.D. Including probable large events B, C, and D with events Z, X, V, T, R, and F results in an average interval of 188 ± 10 years for the period 350–1857 A. D. These three calculations all yield average recurrence intervals of about 200 years for large earthquakes.

Now consider the possibility that a large event has thus far escaped detection in the Pallett Creek section. One such event would lower the average interval from 145 to 133 years. Except for events A, B, and C, the evidence for which was in layers beneath earlier excavations, all of the earthquakes now recognized at the site were recognized during the initial study [*Sieh*, 1978*a*], during which only about 150 m^2 of strata were exposed. Nearly 2000 m^2 of additional exposure failed to reveal evidence for another event. The possibility of a large event escaping notice is therefore quite remote unless the evidence for that event is peculiarly concealed. Such concealment might be possible if one event so closely followed a previous event that little or no sediment had accumulated between earthquake horizons. Then the features of two earthquakes would be interpreted as evidence for only one. For example, one could postulate that two magnitude 8 events separated by 1 day or 1 year are represented by event X. The Pallett Creek record is not able to resolve such an issue. However, in the light of historical experience along major strike-slip faults, scenarios involving very close timing of great earthquakes produced by slip on the same fault can be assigned a very low probability.

Another way in which evidence for a large event might be concealed is by the occurrence of two large events during a long period of nondeposition or during deposition of a poorly bedded unit. A hiatus of about 100 years may exist between units 61 and 68 (Figure 4). Thus it is conceivable that evidence for a large event in about 1450 A.D. would be confused with evidence for event T. Also, unit 59 is so massive and discontinuous that some features attributed to event R could actually represent evidence for an event up to 150 years after event R. Although I cannot exclude the possibility that a large event after R or after T has escaped detection, I regard the likelihood to be quite small. One must consider, also, that splitting either event T or R into two equal events would not necessarily decrease the average interval for large events because it would entail reducing event R or T slip to about a half meter, 4 times less than that documented for the great 1857 event and its predecessor, event X. Thus a "hidden" event would result in downgrading T or R to lesser events, which would actually increase the average interval for large events.

In conclusion, reasonable interpretations of the Pallett Creek record constrain the average recurrence interval for large events to be between about 145 and 200 years.

TABLE 4. Recurrence Intervals for the Past 12 Large Earthquakes at Pallett Creek

Interval	Value, years
Z to ?	>127
X to Z	137 ± 50
V to X	170 ± 86
T to V	200 ± 86
R to T	270 ± 82
N to R	65 ± 119
I to N	80 ± 131
F to I	90 ± 113
D to F	110 ± 99
C to D	145 ± 81
B to C	240 ± 97
A to B	90 ± 120

TABLE 5. Estimated Probabilities of a Large Earthquake Based Upon Various Models of Recurrence and a Variety of Distribution Functions

Model	In 1984	By 2000	Within Next 50 Years
I (200 yrs)	0.3–0.5	7–9	26–34
II (145 yrs)	1–2	21–26	64–67
III (100 yrs)	4–5	49–60	89–98

In percent.

5.3. *Other Considerations*

In order to use effectively an average recurrence interval of 145–200 years to calculate annual or decadal probabilities of occurrence of a large earthquake, something must be known about the distribution of the individual intervals about the mean. On the one hand, the dates of individual earthquakes are so imprecisely determined in this study that very little can be said about this distribution except that individual intervals of large events may range from about a half to two and a half centuries. On the other hand, these data are not contradicted by scenarios in which individual intervals are nearly identical. Worldwide experience with repeated large earthquakes suggests that deviations of 20–45% from the average interval is to be expected [*Sieh*, 1981, p. 182].

Let me complicate interpretation of the Pallett Creek data still more. Assuming that intervals between great earthquakes at Pallett Creek are normally distributed about a mean of 145 or 200 years may be inappropriate and misleading. The data of Table 4 and Figure 16 suggest that the interval may have been decreasing monotonically since event R, about 900 years ago. From Figure 16 one can also speculate that an earlier period of monotonically decreasing intervals occurred between event B and event R. One reasonable view is that the error limits show that the patterns must be coincidental. Another possibility is that the pattern is real and the error limits are much too conservative. The important point is that systematic changes in recurrence interval may be occurring as a function of time.

5.4. *Probabilities of a Future Large Earthquake at Pallett Creek*

In light of the discussion above, three models seem to represent a reasonable spectrum of possibilities at Pallett Creek. In model I the average recurrence interval is about 200 years with individual intervals distributed within 30% of this average but not in any sequential pattern. In a similar model, model II, the average recurrence interval is only 145 years. In a third model, model III, individual intervals have been decreasing monotonically from 270 to 137 years since 1080 A.D., and the best estimate for the occurrence of the next event is only 100 years after 1857. In this model we also assume that a deviation of 30% from this value is possible.

D. R. Brillinger et al. (manuscript in preparation, 1984) have determined probabilities of a large earthquake based upon the

various assumptions of these models using normal, lognormal, Weibull, and other reasonable distribution functions. Table 5 presents the ranges of these preliminary results. From this it is apparent that the likelihood of a large event in the near future is extremely sensitive to the model used. Note, for example, that the chances of a large event by the year 2000 range between 7 and 60%. The imprecision in the dates of the earthquakes recorded at Pallett Creek does not allow us to constrain the possibilities more narrowly. More precise dates and better understanding of the geographical extent of each rupture event will indeed be necessary before probabilistic estimates can be improved substantially.

Acknowledgments. This paper is based on field studies conducted during the summers of 1979 and 1980. Assisting me in the field were Ari Fuad, Christopher Finch, Kristian Meisling, Ronald Miller, Christopher Sanders, Laurie Sieh, and Stuart Stephens. Most of the excavations were dug by equipment operators Jerry Goodman and Chuck Pattison. Access to the property was graciously granted by the owners George and Adele Nickel. Very helpful criticisms of earlier manuscripts were given by Clarence Allen, David Brillinger, Malcolm Clark, Art Darrow, Jim Lienkemper, Art McGarr, Carol Prentice, and Pat Williams. Most of the drafting was done by Kathi Kronenfield. This study was supported by the National Earthquake Hazards Reduction Program, U.S. Geological Survey contract 14-08-0001-16774, 18385, and 19756. Contribution 3823, Division of Geological and Planetary Sciences, California Institute of Technology.

REFERENCES

Barrows, A., Geology and fault activity of the Valyermo segment of the San Andreas fault zone, Los Angeles County, California, *Open File Rep. 79-1-LA*, 49 pp., Calif. Div. of Mines and Geol., Sacramento, 1979.

Barrows, A., Geologic map of the San Andreas fault zone and adjoining terrane, Juniper Hills and vicinity, Los Angeles County, California, *Open File Rep. 80-2-LA*, Calif. Div. of Mines and Geol., Sacramento, 1980.

Broecker, W., Lamont radiocarbon measurements, VI, *Radiocarbon, 1*, 111–132, 1959.

Broecker, W., and Olson, E., Lamont radiocarbon measurements, VIII, *Radiocarbon, 3*, 176–204, 1961.

Damon, P., A. Long, and E. Wallick, Dendrochronologic calibration of the carbon 14 time scale, *Proc. Int. Conf. Radiocarbon Dating, 8th*(1), 45–59, 1972.

Long, A., and B. Rippeteau, Testing contemporaneity and averaging radiocarbon dates, *Am. Antiq., 39*, 205–215, 1974.

Meisling, K., Possible emplacement history of a sandblow structure at Pallett Creek, California, in *Geological Excursions in the Southern California Area*, edited by P. L. Abbott, pp. 63–66, Department of Geological Sciences, San Diego State University, San Diego, Calif., 1980.

Sieh, K., Late Holocene displacement history along the south-central reach of the San Andreas fault, Ph.D. dissertation, 219 pp., Stanford Univ., Stanford, Calif., 1977.

Sieh, K., Prehistoric large earthquakes produced by slip on the San Andreas fault at Pallett Creek, California, *J. Geophys. Res., 83*, 3907–3939, 1978*a*.

Sieh, K., Slip along the San Andreas fault associated with the great 1857 earthquake, *Bull. Seismol. Soc. Am., 68*, 1421–1428, 1978*b*.

Sieh, K., A review of geological evidence for recurrence times of large earthquakes, in *Earthquake Prediction, An International Review, Maurice Ewing Ser.*, vol 4, edited by D. W. Simpson and P. G. Richards, pp. 209–216, AGU, Washington, D. C., 1981.

Sieh, K., and R. Jahns, Holocene activity of the San Andreas fault at Wallace Creek, California, *Geol. Soc. Am. Bull., 95*, in press, 1984.

Stuiver, M., A high-precision calibration of the AD radiocarbon time scale, *Radiocarbon, 24*, 1–26, 1982.

K. E. Sieh, Division of Geological and Planetary Sciences, California Institute of Technology, Pasadena, CA 91125.

(Received November 7, 1983;
revised March 29, 1984;
accepted April 17, 1984.)